Available online at www.sciencedirect.com
SCIENCE DIRECT®
Comput. Methods Appl. Mech. Engrg. 193 (2004) 5301–5338
Computer methods in applied mechanics and engineering
www.elsevier.com/locate/cma

Cam-Clay plasticity. Part V: A mathematical framework for three-phase deformation and strain localization analyses of partially saturated porous media

Ronaldo I. Borja *

Department of Civil and Environmental Engineering, Stanford University, Stanford, CA 94305-4020, USA

Received 30 August 2003; received in revised form 22 December 2003; accepted 22 December 2003

Abstract

We present a mathematical framework for deformation and strain localization analyses of partially saturated granular media using three-phase continuum mixture theory. First, we develop conservation laws governing a three-phase mixture to identify energy-conjugate expressions for constitutive modeling. Energy conjugate expressions identified relate a certain measure of effective stress to the deformation of the solid matrix, the degree of saturation to the matrix suction, the pressure in each phase to the corresponding intrinsic volume change of this phase, and the seepage forces to the corresponding pressure gradients. From the second of law of thermodynamics we obtain the dissipation inequality; from the principle of maximum plastic dissipation we derive a condition for the convexity of the yield function. Then, we formulate expressions describing conditions for the onset of tabular deformation bands under locally drained and locally undrained conditions. Finally, we cast a specific constitutive model for partially saturated soils within the proposed mathematical framework, and implement it in the context of return mapping algorithm of computational plasticity. The proposed constitutive model degenerates to the classical modified Cam-Clay model of soil mechanics in the limit of full saturation. Numerical examples are presented to demonstrate the performance of the return mapping algorithm as well as illustrate the localization properties of the model as functions of imposed deformation and matrix suction histories.

Keyword: Cam-Clay plasticity

* Fax: +650 723 7514.
E-mail address: borja@stanford.edu

0045-7825/$ - see front matter © 2004 Elsevier B.V. All rights reserved.
doi:10.1016/j.cma.2003.12.067

1. Introduction

Porous media consist of three separate phases: solid, liquid, and gas. Description of the deformation and movement/transport of both liquid and gas relative to the solid phase, and the deformation of the solid matrix itself, is one of the most challenging aspects of multiphase mechanics. In geology, the topmost layer of the earth's crust comprises a three-phase system called the unsaturated, or partially saturated, zone. In the western United States the unsaturated zone can be more than a hundred meters thick, whereas in wetlands it may fluctuate seasonally or not exist at all [1]. Where an unsaturated zone exists, proper treatment of the significant variables and phenomena affecting its behavior, such as capillary flow, adsorption, chemical potential, and temperature, must all be considered whenever possible. Prediction of the mechanical behavior of unsaturated zones is crucial for the construction of underground structures, such as tunneling by compressed air [2,3].

Mechanical models for partially saturated soils must encompass models applicable to fully saturated soils in the limit as the degree of saturation approaches unity. This has motivated much work extending classical plasticity models for fully saturated soils to include additional variables reflecting the relevant phenomena associated with partial saturation, such as the surface tension induced by the presence of water meniscus surrounding two contacting solid grains. There seems to be a universal consensus that for constitutive modeling purposes these phenomena may be lumped into a macroscopic variable called the matrix suction, defined as the difference between the pore air and pore water pressures in the void (see e.g., the editorial of Thomas [4]). Energy consideration provides support for this idea, at least from a continuum standpoint, as well as elucidates possible definitions for a constitutive effective stress conjugate to the macroscopic deformation of the solid matrix. Possible constitutive effective stresses include the net stress and the Bishop stress [5–15].

Like many other engineering materials undergoing non-homogeneous deformation, partially saturated granular media can also exhibit localized deformation behavior leading to rapid loss of shear strength. For example, instabilities on moraine slopes have been reported in [16] due to loss of suction. Similar phenomena have been described in [17–20] associated with rainfall-induced loss of shear strength in partially saturated slopes. Although material instability as a whole generally covers a wide range of possible failure modes and thus is beyond the scope of this paper, we address in this work one type of failure mode, that associated with the formation of a tabular deformation band. For one-phase materials bifurcation theory may be used to detect the onset of a deformation band [21–23] largely responsible for loss of shear strength. In fully saturated geomaterials the presence of fluids in the voids is known to influence the associated localized deformation behavior [24–26], and is thus typically analysed using some definitions of effective stress for constitutive modeling purposes, such as the Terzaghi stress [27] and the Nur-Byerlee stress [28]. For partially saturated media, however, such decomposition of the total stress is not so obvious. Unfortunately, however the total stress is decomposed plays a key role in the assessment of the so-called drained and undrained deformation and strain localization responses of geomaterials [29–31].

In this paper we describe a mathematical framework for three-phase deformation and strain localization modeling of partially saturated granular media. The paper begins with a presentation of the master balance laws. From balance of energy we identify work-conjugate expressions suitable for constitutive modeling. Energy conjugate expressions identified relate a certain measure of effective stress to the deformation of the solid matrix, the degree of saturation to the matrix suction, the pressure in each phase to the corresponding intrinsic volume change of this phase, and the seepage forces to the corresponding pressure gradients. With these results, we then use the second law of thermodynamics to obtain an expression for the reduced dissipation inequality; the principle of maximum plastic dissipation then leads to the convexity condition for the yield surface. Furthermore, using this framework we formulate essential conditions for the emergence of a shear band for three-phase media under the extreme cases of fully drained and fully undrained conditions. As usual, these localization conditions require continuity of the total traction vector

across a surface of discontinuity. Undrained and drained localizations are herein treated with and without jumps in the pore air and pore pressure fields, respectively.

As a specific example, we formulate analytically and implement numerically a two-invariant Cam-Clay-type plasticity model for partially saturated soils. It must be noted that constitutive models for partially saturated soils are now only coming of age, and much work remains to be done to improve on and calibrate these models. The goal of the formulation and implementation of this specific plasticity model is not to advocate its use per se, but rather to illustrate how more robust models, such as a three-invariant Cam-Clay model [32,33], can be implemented within the proposed mathematical framework. For the numerical implementation of the plasticity model considered in this work, we utilize a return mapping algorithm in the elastic strain invariant space advocated in [34,35]. Remarkably, the numerical implementation requires only modest extension of the traditional Cam-Clay-type plasticity formulation for fully saturated soils [36–39], suggesting the potential of the proposed framework for accommodating more complex elastoplastic models.

Notations and symbols used in this paper are as follows: bold-face letters denote tensors and vectors; the symbol ' . ' denotes an inner product of two vectors (e.g. $\boldsymbol{a}\cdot\boldsymbol{b}=a_ib_i$), or a single contraction of adjacent indices of two tensors (e.g. $\boldsymbol{c}\cdot\boldsymbol{d}=c_{ij}d_{jk}$); the symbol ':' denotes an inner product of two second-order tensors (e.g. $\boldsymbol{c}:\boldsymbol{d}=c_{ij}d_{ij}$), or a double contraction of adjacent indices of tensors of rank two and higher (e.g. $\boldsymbol{C}:\boldsymbol{\epsilon}^{\mathrm{e}}=C_{ijkl}\epsilon^{\mathrm{e}}_{kl}$); the symbol '$\otimes$' denotes a juxtaposition, e.g., $(\boldsymbol{a}\otimes\boldsymbol{b})_{ij}=a_ib_j$; and for any symmetric second order tensors $\boldsymbol{\alpha}$ and $\boldsymbol{\beta}$, $(\boldsymbol{\alpha}\otimes\boldsymbol{\beta})_{ijkl}=\alpha_{ij}\beta_{kl}$.

2. Conservation laws

We consider a three-phase mixture composed of a solid matrix whose voids are continuous and filled with water and air. The solid matrix, or skeleton, plays a special role in the mathematical description in that it defines the volume of the mixture, herein written in the current configuration as $V=V_{\mathrm{s}}+V_{\mathrm{w}}+V_{\mathrm{a}}$. The corresponding total masses are $M=M_{\mathrm{s}}+M_{\mathrm{w}}+M_{\mathrm{a}}$, where $M_\alpha=\rho_\alpha V_\alpha$ for $\alpha=$ solid, water, and air; and ρ_α is the true mass density of the α phase. The volume fraction occupied by the α phase is given by $\phi^\alpha=V_\alpha/V$, and thus

$$\phi^{\mathrm{s}}+\phi^{\mathrm{w}}+\phi^{\mathrm{a}}=1. \tag{2.1}$$

The partial mass density of the α phase is given by $\rho^\alpha=\phi^\alpha\rho_\alpha$, and thus

$$\rho^{\mathrm{s}}+\rho^{\mathrm{w}}+\rho^{\mathrm{a}}=\rho, \tag{2.2}$$

where $\rho=M/V$ is the total mass density of the mixture. As a general notation, phase designations in the superscript form pertain to average or partial quantities; and in the subscript form to intrinsic or true quantities.

2.1. Balance of mass

In writing out the mass balance equations for a three-phase mixture, a key point is to focus on the current configuration of the mixture and describe the motions of the water and air phases relative to the motion of the solid phase. We denote the instantaneous intrinsic velocities of the solid, water and air phases by $\boldsymbol{v}$, $\boldsymbol{v}_{\mathrm{w}}$, and $\boldsymbol{v}_{\mathrm{a}}$, respectively, and the total time-derivative following the solid phase motion by

$$\frac{\mathrm{d}(\cdot)}{\mathrm{d}t}=\frac{\partial(\cdot)}{\partial t}+\mathrm{grad}(\cdot)\cdot\boldsymbol{v}.$$

Ignoring mass exchanges among the three phases, balance of mass for the solid, water, and air phases then write [31]

$$\frac{\mathrm{d}\rho^{\mathrm{s}}}{\mathrm{d}t} + \rho^{\mathrm{s}}\mathrm{div}(\boldsymbol{v}) = 0, \tag{2.3a}$$

$$\frac{\mathrm{d}\rho^{\mathrm{w}}}{\mathrm{d}t} + \rho^{\mathrm{w}}\mathrm{div}(\boldsymbol{v}) = -\mathrm{div}(\boldsymbol{w}^{\mathrm{w}}), \tag{2.3b}$$

$$\frac{\mathrm{d}\rho^{\mathrm{a}}}{\mathrm{d}t} + \rho^{\mathrm{a}}\mathrm{div}(\boldsymbol{v}) = -\mathrm{div}(\boldsymbol{w}^{\mathrm{a}}). \tag{2.3c}$$

Here, $\boldsymbol{w}^{\alpha}$ (for α = water, air) is the Eulerian relative flow vector of the α phase with respect to the solid matrix, given explicitly by the relations

$$\boldsymbol{w}^{\alpha} = \rho^{\alpha}\tilde{\boldsymbol{v}}_{\alpha}, \quad \tilde{\boldsymbol{v}}_{\alpha} = \boldsymbol{v}_{\alpha} - \boldsymbol{v}, \quad \alpha = \mathrm{w}, \mathrm{a}. \tag{2.4}$$

The flow vector $\boldsymbol{w}^{\alpha}$ has the physical significance that its scalar product with the unit normal vector $\boldsymbol{n}$ to a unit surface area attached to the solid matrix is the mass flux J^{α} of the α phase relative to the solid matrix flowing across the same unit area, i.e.,

$$\boldsymbol{w}^{\alpha} \cdot \boldsymbol{n} = J^{\alpha}, \quad \alpha = \mathrm{w}, \mathrm{a}. \tag{2.5}$$

Thus,

$$m^{\alpha} = \int_A J^{\alpha}\,\mathrm{d}A = \int_A \boldsymbol{w}^{\alpha} \cdot \boldsymbol{n}\,\mathrm{d}A = \int_V \mathrm{div}(\boldsymbol{w}^{\alpha})\,\mathrm{d}V \tag{2.6}$$

represents the net mass flux of the α phase on the total volume V, and the terms on the right-hand side of (2.3b,c) are thus the localizations of these mass fluxes to a material point attached to the solid matrix. If there is no relative motion between the α phase and the solid phase such that the mass M_{α} contained in the volume V moves exactly with the solid matrix, then $\tilde{\boldsymbol{v}}_{\alpha} = \boldsymbol{0}$ and $\boldsymbol{w}^{\alpha} = \boldsymbol{0}$. It is, however, possible that $m^{\alpha} = 0$ even if $\boldsymbol{w}^{\alpha} \neq \boldsymbol{0}$ provided that the latter is divergence-free; in this case the net mass flux is zero as a result of the α phase material being displaced by another α phase material of the same mass quantity.

For barotropic flows a functional relationship of the form $f(p_{\alpha}, \rho_{\alpha}) = 0$ exists for each phase [40], where p_{α} denotes the intrinsic pressure equal to the actual force per unit actual area acting on the α phase. Thus we can write

$$\frac{\mathrm{d}\rho_{\alpha}}{\mathrm{d}t} = \rho'_{\alpha}(p_{\alpha})\frac{\mathrm{d}p_{\alpha}}{\mathrm{d}t}, \tag{2.7}$$

where the prime denotes ordinary differentiation, and so,

$$\frac{\mathrm{d}\rho^{\alpha}}{\mathrm{d}t} = \frac{\mathrm{d}(\phi^{\alpha}\rho_{\alpha})}{\mathrm{d}t} = \phi^{\alpha}\rho'_{\alpha}(p_{\alpha})\frac{\mathrm{d}p_{\alpha}}{\mathrm{d}t} + \rho_{\alpha}\frac{\mathrm{d}\phi^{\alpha}}{\mathrm{d}t}. \tag{2.8}$$

Denoting the bulk modulus of the α phase as

$$K_{\alpha} = \rho_{\alpha}p'_{\alpha}(\rho_{\alpha}), \quad \alpha = \mathrm{s}, \mathrm{w}, \mathrm{a}, \tag{2.9}$$

the mass balance equations then become

$$\frac{\mathrm{d}\phi^{\mathrm{s}}}{\mathrm{d}t} + \frac{\phi^{\mathrm{s}}}{K_{\mathrm{s}}}\frac{\mathrm{d}p_{\mathrm{s}}}{\mathrm{d}t} + \phi^{\mathrm{s}}\mathrm{div}(\boldsymbol{v}) = 0, \tag{2.10a}$$

$$\frac{\mathrm{d}\phi^{\mathrm{w}}}{\mathrm{d}t} + \frac{\phi^{\mathrm{w}}}{K_{\mathrm{w}}}\frac{\mathrm{d}p_{\mathrm{w}}}{\mathrm{d}t} + \phi^{\mathrm{w}}\mathrm{div}(\boldsymbol{v}) = -\frac{1}{\rho_{\mathrm{w}}}\mathrm{div}(\boldsymbol{w}^{\mathrm{w}}), \tag{2.10b}$$

$$\frac{\mathrm{d}\phi^{\mathrm{a}}}{\mathrm{d}t}+\frac{\phi^{\mathrm{a}}}{K_{\mathrm{a}}}\frac{\mathrm{d}p_{\mathrm{a}}}{\mathrm{d}t}+\phi^{\mathrm{a}}\mathrm{div}(\boldsymbol{v})=-\frac{1}{\rho_{\mathrm{a}}}\mathrm{div}(\boldsymbol{w}^{\mathrm{a}}). \tag{2.10c}$$

Next let us introduce void fractions ψ^{w} and ψ^{a}, defined as the ratio between the volume of the α phase in the void to the volume of the void itself,

$$\psi^{\mathrm{w}}=\frac{V_{\mathrm{w}}}{V_{\mathrm{w}}+V_{\mathrm{a}}}=\frac{\phi^{\mathrm{w}}}{1-\phi^{\mathrm{s}}},\quad \psi^{\mathrm{a}}=\frac{V_{\mathrm{a}}}{V_{\mathrm{w}}+V_{\mathrm{a}}}=\frac{\phi^{\mathrm{a}}}{1-\phi^{\mathrm{s}}},\quad \psi^{\mathrm{w}}+\psi^{\mathrm{a}}=1. \tag{2.11}$$

In geotechnical literature, ψ^{w} is commonly denoted as the degree of saturation S_r, and $\psi^{\mathrm{a}}=1-S_r$, but we shall use the void fractions herein for simplicity in the notation. Taking the material time derivative with respect to the solid phase motion, we obtain

$$\frac{\mathrm{d}\phi^{\alpha}}{\mathrm{d}t}=(1-\phi^{\mathrm{s}})\frac{\mathrm{d}\psi^{\alpha}}{\mathrm{d}t}-\psi^{\alpha}\frac{\mathrm{d}\phi^{\mathrm{s}}}{\mathrm{d}t}=(1-\phi^{\mathrm{s}})\frac{\mathrm{d}\psi^{\alpha}}{\mathrm{d}t}+\psi^{\alpha}\left[\frac{\phi^{\mathrm{s}}}{K_{\mathrm{s}}}\frac{\mathrm{d}p_{\mathrm{s}}}{\mathrm{d}t}+\phi^{\mathrm{s}}\mathrm{div}(\boldsymbol{v})\right],\quad \alpha=\mathrm{w},\mathrm{a}, \tag{2.12}$$

where the second equality follows from balance of mass for the solid phase, (2.10a). Thus, balance of mass for the water and air phases, (2.10b,c), can be rewritten as

$$(1-\phi^{\mathrm{s}})\frac{\mathrm{d}\psi^{\alpha}}{\mathrm{d}t}+\frac{\phi^{\alpha}}{K_{\alpha}}\frac{\mathrm{d}p_{\alpha}}{\mathrm{d}t}+\frac{\psi^{\alpha}\phi^{\mathrm{s}}}{K_{\mathrm{s}}}\frac{\mathrm{d}p_{\mathrm{s}}}{\mathrm{d}t}+\psi^{\alpha}\mathrm{div}(\boldsymbol{v})=-\frac{1}{\rho_{\alpha}}\mathrm{div}(\boldsymbol{w}^{\alpha}). \tag{2.13}$$

By definition, a fully saturated case corresponds to $\phi^{\mathrm{a}}=\psi^{\mathrm{a}}=0$, and the above equation is non-trivial only for the water phase. Further, if both the solid and water constituent phases are incompressible the above equation reduces to $\mathrm{div}(\boldsymbol{v})+\mathrm{div}(\tilde{\boldsymbol{v}}^{\mathrm{w}})=0$, where $\tilde{\boldsymbol{v}}^{\mathrm{w}}=\phi^{\mathrm{w}}\tilde{\boldsymbol{v}}_{\mathrm{w}}$ is often called the superficial Darcy velocity and $\tilde{\boldsymbol{v}}_{\mathrm{w}}$ is the true seepage velocity. Except for the assumption of barotropic flows, note that the above formulation is perfectly general and includes the compressibilities of all the constituent phases.

2.2. Balance of momentum

Let $\boldsymbol{\sigma}^{\alpha}$ denote the Cauchy partial stress tensor for the α phase, with α = solid, water, and air. The total Cauchy stress tensor $\boldsymbol{\sigma}$ is obtained from the sum

$$\boldsymbol{\sigma}=\boldsymbol{\sigma}^{\mathrm{s}}+\boldsymbol{\sigma}^{\mathrm{w}}+\boldsymbol{\sigma}^{\mathrm{a}}. \tag{2.14}$$

In the above equation we ignore the stress arising from the presence of a meniscus, identified by Fredlund and Morgenstern [5] as the 'contractile skin' stress and subsequently considered by Houlsby [41] as the fourth-phase stress. We also define the first Piola–Kirchhoff partial stress tensor $\boldsymbol{P}^{\alpha}=J\boldsymbol{\sigma}^{\alpha}\cdot\boldsymbol{F}^{-\mathrm{t}}$, where $J=\det(\boldsymbol{F})$ is the jacobian and $\boldsymbol{F}$ is the deformation gradient of the solid phase motion. The total first Piola–Kirchhoff stress tensor is then given by

$$\boldsymbol{P}=\boldsymbol{P}^{\mathrm{s}}+\boldsymbol{P}^{\mathrm{w}}+\boldsymbol{P}^{\mathrm{a}}. \tag{2.15}$$

Balance of linear momentum for the α phase may be expressed through the alternative expressions

$$\mathrm{div}(\boldsymbol{\sigma}^{\alpha})+\rho^{\alpha}\mathbf{g}+\boldsymbol{h}^{\alpha}=\rho^{\alpha}\frac{\mathrm{d}^{\alpha}\boldsymbol{v}_{\alpha}}{\mathrm{d}t}, \tag{2.16a}$$

$$\mathrm{DIV}(\boldsymbol{P}^{\alpha})+J\rho^{\alpha}\mathbf{g}+\boldsymbol{H}^{\alpha}=J\rho^{\alpha}\frac{\mathrm{d}^{\alpha}\boldsymbol{v}_{\alpha}}{\mathrm{d}t}, \tag{2.16b}$$

for α = s, w, a; where $\mathbf{g}$ is the vector of gravity accelerations, $\boldsymbol{h}^{\alpha}$ is the resultant body force per unit current volume of the solid matrix exerted on the α phase; $\boldsymbol{H}^{\alpha}=J\boldsymbol{h}^{\alpha}$ is the corresponding resultant body force per unit reference volume of the solid matrix; and div and DIV are the divergence operators evaluated with

respect to the current and reference configurations, respectively. The operator $\mathrm{d}^\alpha(\cdot)/\mathrm{d}t$ denotes a material time derivative following the α phase motion and is related to the operator $\mathrm{d}(\cdot)/\mathrm{d}t$ via the relation

$$\frac{\mathrm{d}^\alpha(\cdot)}{\mathrm{d}t} = \frac{\mathrm{d}(\cdot)}{\mathrm{d}t} + \mathrm{grad}(\cdot)\cdot\tilde{\boldsymbol{v}}_\alpha.$$

Furthermore, the forces $\boldsymbol{h}^\alpha$ and $\boldsymbol{H}^\alpha$ are internal to the mixture and thus satisfy the relations $\boldsymbol{h}^{\mathrm{s}} + \boldsymbol{h}^{\mathrm{w}} + \boldsymbol{h}^{\mathrm{a}} = \boldsymbol{H}^{\mathrm{s}} + \boldsymbol{H}^{\mathrm{w}} + \boldsymbol{H}^{\mathrm{a}} = \boldsymbol{0}$.

Adding (2.16) for all the three phases, we obtain the balance of momentum for the entire mixture expressed in the alternative forms

$$\mathrm{div}(\boldsymbol{\sigma}) + \rho\mathbf{g} = \sum_{\alpha=\mathrm{s,w,a}} \rho^\alpha \frac{\mathrm{d}^\alpha \boldsymbol{v}_\alpha}{\mathrm{d}t}, \tag{2.17a}$$

$$\mathrm{DIV}(\boldsymbol{P}) + \rho_0\mathbf{g} = \sum_{\alpha=\mathrm{s,w,a}} J\rho^\alpha \frac{\mathrm{d}^\alpha \boldsymbol{v}_\alpha}{\mathrm{d}t}, \tag{2.17b}$$

where $\rho_0 = J\rho$ is the pull-back mass density of the mixture in the reference configuration. Note that the solid phase material now at point $\boldsymbol{x}$ in the current configuration is the same solid phase material originally at the point $\boldsymbol{X}$ in the reference configuration, but the water and air phases at $\boldsymbol{x}$ and $\boldsymbol{X}$ are not the same material points. Hence, the total reference mass density ρ_0 in V_0 is not conserved by ρ in V. Now, if we rewrite the equations of motion relative to the motion of the solid matrix, then balance of momentum for the entire mixture becomes

$$\mathrm{div}(\boldsymbol{\sigma}) + \rho\mathbf{g} = \rho\frac{\mathrm{d}\boldsymbol{v}}{\mathrm{d}t} + \sum_{\alpha=\mathrm{w,a}} \rho^\alpha \left[\frac{\mathrm{d}\tilde{\boldsymbol{v}}_\alpha}{\mathrm{d}t} + \mathrm{grad}(\boldsymbol{v}_\alpha)\cdot\tilde{\boldsymbol{v}}_\alpha\right], \tag{2.18a}$$

$$\mathrm{DIV}(\boldsymbol{P}) + \rho_0\mathbf{g} = \rho_0\frac{\mathrm{d}\boldsymbol{v}}{\mathrm{d}t} + \sum_{\alpha=\mathrm{w,a}} J\rho^\alpha \left[\frac{\mathrm{d}\tilde{\boldsymbol{v}}_\alpha}{\mathrm{d}t} + \mathrm{grad}(\boldsymbol{v}_\alpha)\cdot\tilde{\boldsymbol{v}}_\alpha\right]. \tag{2.18b}$$

A complete formulation for the dynamic problem then requires the specification of either: (a) the motions of the three phases, or (b) the motion of the solid phase together with the relative motions of the water and air phases to that of the solid phase, see [29,30].

2.3. Balance of energy

Let $\mathscr{K}$ be the kinetic energy and $\mathscr{I}$ be the internal energy of a three-phase mixture contained in a volume V. The first law of thermodynamics states that

$$\frac{\mathrm{D}\mathscr{K}}{\mathrm{D}t} + \frac{\mathrm{D}\mathscr{I}}{\mathrm{D}t} = \mathscr{P}, \tag{2.19}$$

where $\mathscr{P}$ is the total power and the symbol $\mathrm{D}(\cdot)/\mathrm{D}t$ denotes a total material time derivative. For a three-phase mixture the total kinetic energy is given by

$$\mathscr{K} = \sum_{\alpha=\mathrm{s,w,a}} \int_V \frac{1}{2}\rho^\alpha \boldsymbol{v}_\alpha\cdot\boldsymbol{v}_\alpha\,\mathrm{d}V. \tag{2.20}$$

The time rate of change is obtained as

$$\frac{\mathrm{D}\mathscr{K}}{\mathrm{D}t} = \sum_{\alpha=\mathrm{s,w,a}} \frac{\mathrm{d}^\alpha}{\mathrm{d}t}\int_V \frac{1}{2}\rho^\alpha \boldsymbol{v}_\alpha\cdot\boldsymbol{v}_\alpha\,\mathrm{d}V = \int_V \sum_{\alpha=\mathrm{s,w,a}} \left(\rho^\alpha \frac{\mathrm{d}^\alpha \boldsymbol{v}_\alpha}{\mathrm{d}t}\right)\cdot\boldsymbol{v}_\alpha\,\mathrm{d}V \tag{2.21}$$

Note that the total material time derivative is obtained as the sum of the material derivatives of the individual phases.

The total power $\mathscr{P}$ is the sum of the mechanical and non-mechanical powers. Our primary goal here is to develop work conjugate expressions for the constitutive modeling of the mechanical behavior of three-phase media, so we shall ignore the non-mechanical power in what follows (the reader is referred to [31,42] for a more complete treatment including non-mechanical power). The mechanical power is the sum of the powers of the surface tractions and the body forces, and for a three-phase medium we have

$$\mathscr{P} = \int_A \sum_{\alpha=\mathrm{s,w,a}} \boldsymbol{\sigma}^\alpha : \boldsymbol{n} \otimes \boldsymbol{v}_\alpha \,\mathrm{d}A + \int_V \sum_{\alpha=\mathrm{s,w,a}} (\boldsymbol{h}^\alpha \cdot \boldsymbol{v}_\alpha + \rho^\alpha \mathbf{g} \cdot \boldsymbol{v}_\alpha)\,\mathrm{d}V, \tag{2.22}$$

where A is the surface area of the volume V, and $\boldsymbol{n}$ is the unit outward normal vector to $\mathrm{d}A$. The surface integral can be converted into a volume integral using Gauss theorem, yielding the following result

$$\begin{aligned}\mathscr{P} &= \int_V \sum_{\alpha=\mathrm{s,w,a}} [\mathrm{div}(\boldsymbol{\sigma}^\alpha \cdot \boldsymbol{v}_\alpha) + \boldsymbol{h}^\alpha \cdot \boldsymbol{v}_\alpha + \rho^\alpha \mathbf{g} \cdot \boldsymbol{v}_\alpha]\,\mathrm{d}V \\ &= \int_V \sum_{\alpha=\mathrm{s,w,a}} [\boldsymbol{\sigma}^\alpha : \boldsymbol{l}_\alpha + \mathrm{div}(\boldsymbol{\sigma}^\alpha) \cdot \boldsymbol{v}_\alpha + \boldsymbol{h}^\alpha \cdot \boldsymbol{v}_\alpha + \rho^\alpha \mathbf{g} \cdot \boldsymbol{v}_\alpha]\,\mathrm{d}V,\end{aligned} \tag{2.23}$$

where $\boldsymbol{l}_\alpha = \mathrm{grad}(\boldsymbol{v}_\alpha)$ is the spatial velocity gradient of the α phase motion. Subtracting $\mathrm{D}\mathscr{K}/\mathrm{D}t$ and using the balance of momentum (2.16) yields

$$\frac{\mathrm{D}\mathscr{I}}{\mathrm{D}t} = \mathscr{P} - \frac{\mathrm{D}\mathscr{K}}{\mathrm{D}t} = \int_V \sum_{\alpha=\mathrm{s,w,a}} \boldsymbol{\sigma}^\alpha : \boldsymbol{l}_\alpha \,\mathrm{d}V = \int_V \sum_{\alpha=\mathrm{s,w,a}} \boldsymbol{\sigma}^\alpha : \boldsymbol{d}_\alpha \,\mathrm{d}V, \tag{2.24}$$

where $\boldsymbol{d}_\alpha = \mathrm{sym}(\boldsymbol{l}_\alpha)$ is the rate of deformation tensor for the α phase. The expression inside the volume integral sign is the internal power per unit current volume,

$$\frac{\mathrm{De}}{\mathrm{D}t} = \sum_{\alpha=\mathrm{s,w,a}} \boldsymbol{\sigma}^\alpha : \boldsymbol{l}_\alpha = \sum_{\alpha=\mathrm{s,w,a}} \boldsymbol{\sigma}^\alpha : \boldsymbol{d}_\alpha. \tag{2.25}$$

The above result agrees with a similar expression presented in [43] for a fully saturated solid–water mixture.

In developing constitutive theories for a three-phase mixture a possible approach would be to relate an objective rate expression for $\boldsymbol{\sigma}^\alpha$ with its work-conjugate tensor $\boldsymbol{d}_\alpha$ in view of the above structure of $\mathrm{De}/\mathrm{D}t$. An alternative approach would be to determine other possible constitutive stresses that are also work-conjugate to the velocity gradient of the solid matrix motion. We pursue the latter approach by first rewriting (2.25) in the form

$$\frac{\mathrm{De}}{\mathrm{D}t} = \boldsymbol{\sigma} : \boldsymbol{l} + \sum_{\alpha=\mathrm{w,a}} \boldsymbol{\sigma}^\alpha : \tilde{\boldsymbol{l}}_\alpha, \quad \tilde{\boldsymbol{l}}_\alpha = \boldsymbol{l}_\alpha - \boldsymbol{l}, \tag{2.26}$$

where $\boldsymbol{l} \equiv \boldsymbol{l}_\mathrm{s}$. The latter expression can be obtained simply by adding the null expression $(\boldsymbol{\sigma} - \boldsymbol{\sigma}^\mathrm{s} - \boldsymbol{\sigma}^\mathrm{w} - \boldsymbol{\sigma}^\mathrm{a}) : \boldsymbol{l}$ to (2.25).

Next we exploit the isotropic nature of the partial stress tensors $\boldsymbol{\sigma}^\mathrm{w}$ and $\boldsymbol{\sigma}^\mathrm{a}$ and write them more specifically as

$$\boldsymbol{\sigma}^\mathrm{w} = -\phi^\mathrm{w} p_\mathrm{w} \mathbf{1}, \quad \boldsymbol{\sigma}^\mathrm{a} = -\phi^\mathrm{a} p_\mathrm{a} \mathbf{1}, \tag{2.27}$$

where p_w and p_a are the intrinsic pore water and pore air pressures, respectively, as defined before, and $\mathbf{1}$ is the second-order identity tensor. The internal power per unit volume can then be written as

$$\frac{\mathrm{De}}{\mathrm{D}t} = \boldsymbol{\sigma} : \boldsymbol{l} - \sum_{\alpha=\mathrm{w,a}} \phi^{\alpha} p_{\alpha} \mathrm{div}(\tilde{\boldsymbol{v}}_{\alpha}). \tag{2.28}$$

However, we note that the divergence of the Eulerian relative flow vector $\boldsymbol{w}^{\alpha}$ is

$$\mathrm{div}(\boldsymbol{w}^{\alpha}) = \mathrm{div}(\rho^{\alpha}\tilde{\boldsymbol{v}}_{\alpha}) = \mathrm{div}(\phi^{\alpha}\rho_{\alpha}\tilde{\boldsymbol{v}}_{\alpha}) = \phi^{\alpha}\rho_{\alpha}\mathrm{div}(\tilde{\boldsymbol{v}}_{\alpha}) + \tilde{\boldsymbol{v}}_{\alpha} \cdot \mathrm{grad}(\phi^{\alpha}\rho_{\alpha}). \tag{2.29}$$

Substituting (2.29) into (2.13), solving for $\mathrm{div}(\tilde{\boldsymbol{v}}_{\alpha})$, and substituting the final result back into (2.28), we obtain

$$\frac{\mathrm{De}}{\mathrm{D}t} = \boldsymbol{\sigma}' : \boldsymbol{l} + \frac{\mathrm{De}'}{\mathrm{D}t}, \tag{2.30}$$

where $\boldsymbol{\sigma}'$ is a constitutive effective stress that is also work-conjugate to $\boldsymbol{l}$, given explicitly by the relation

$$\boldsymbol{\sigma}' = \boldsymbol{\sigma} + \overline{p}\mathbf{1}, \quad \overline{p} = \sum_{\alpha=\mathrm{w,a}} \psi^{\alpha} p_{\alpha}, \tag{2.31}$$

and

$$\frac{\mathrm{De}'}{\mathrm{D}t} = \sum_{\alpha=\mathrm{w,a}} \left[\frac{1}{\rho_{\alpha}} \tilde{\boldsymbol{v}}_{\alpha} \cdot \mathrm{grad}(\phi^{\alpha}\rho_{\alpha}) + (1-\phi^{\mathrm{s}}) \frac{\mathrm{d}\psi^{\alpha}}{\mathrm{d}t} + \frac{\phi^{\alpha}}{K_{\alpha}} \frac{\mathrm{d}p_{\alpha}}{\mathrm{d}t} + \frac{\psi^{\alpha}\phi^{\mathrm{s}}}{K_{\mathrm{s}}} \frac{\mathrm{d}p_{\mathrm{s}}}{\mathrm{d}t} \right] p_{\alpha}. \tag{2.32}$$

In the fully saturated regime, we have $\psi^{\mathrm{a}} = \phi^{\mathrm{a}} = 0$, $\psi^{\mathrm{w}} = 1$, and $\phi^{\mathrm{w}} + \phi^{\mathrm{s}} = 1$. In this case the constitutive stress reduces to the effective stress of [27],

$$\boldsymbol{\sigma}' = \boldsymbol{\sigma} + p_{\mathrm{w}}\mathbf{1}. \tag{2.33}$$

In the partially saturated regime, we have $\phi^{\mathrm{s}} = 1 - n$, $\phi^{\mathrm{w}} = nS_r$, $\phi^{\mathrm{a}} = n(1 - S_r)$, $\psi^{\mathrm{w}} = S_r$, and $\psi^{\mathrm{a}} = 1 - S_r$, where n is the porosity and S_r is the degree of saturation. The constitutive stress thus reduces to the form

$$\boldsymbol{\sigma}' = \boldsymbol{\sigma} + \overline{p}\mathbf{1}, \quad \overline{p} = S_r p_{\mathrm{w}} + (1 - S_r) p_{\mathrm{a}}. \tag{2.34}$$

The above form of effective stress for the partially saturated case appears to have originated from [44,45].

The first term in $\mathrm{De}'/\mathrm{D}t$ can be written as

$$\frac{\mathrm{De}'_1}{\mathrm{D}t} = \sum_{\alpha=\mathrm{w,a}} \left[\frac{1}{\rho_{\alpha}} \tilde{\boldsymbol{v}}_{\alpha} \cdot \mathrm{grad}(\phi^{\alpha}\rho_{\alpha}) \right] p_{\alpha} = \sum_{\alpha=\mathrm{w,a}} \left[\frac{1}{\rho_{\alpha}} \mathrm{div}(\boldsymbol{w}^{\alpha}) - \phi^{\alpha}\mathrm{div}(\tilde{\boldsymbol{v}}_{\alpha}) \right] p_{\alpha}. \tag{2.35}$$

The second term in $\mathrm{De}'/\mathrm{D}t$ simplifies to

$$\frac{\mathrm{De}'_2}{\mathrm{D}t} = (1-\phi^{\mathrm{s}}) \sum_{\alpha=\mathrm{w,a}} \frac{\mathrm{d}\psi^{\alpha}}{\mathrm{d}t} p_{\alpha} = -ns \frac{\mathrm{d}S_r}{\mathrm{d}t}, \quad s = p_{\mathrm{a}} - p_{\mathrm{w}}. \tag{2.36}$$

Here, s is the suction stress representing the difference between the water and air pressures in the voids. We note that $\mathrm{De}'_2/\mathrm{D}t$ vanishes in the perfectly saturated regime since $S_r = 1 = \text{constant}$. The third term in $\mathrm{De}'/\mathrm{D}t$ represents the effect of the compressibilities of the constituent phases, and if we assume incompressible solid and water phases we get

$$\frac{\mathrm{De}'_3}{\mathrm{D}t} = \sum_{\alpha=\mathrm{w,a}} \left[\frac{\phi^{\alpha}}{K_{\alpha}} \frac{\mathrm{d}p_{\alpha}}{\mathrm{d}t} + \frac{\psi^{\alpha}\phi^{\mathrm{s}}}{K_{\mathrm{s}}} \frac{\mathrm{d}p_{\mathrm{s}}}{\mathrm{d}t} \right] p_{\alpha} = \frac{\phi^{\mathrm{a}}}{K_{\mathrm{a}}} \frac{\mathrm{d}p_{\mathrm{a}}}{\mathrm{d}t} p_{\mathrm{a}} = \frac{\phi^{\mathrm{a}}}{\rho_{\mathrm{a}}} \frac{\mathrm{d}\rho_{\mathrm{a}}}{\mathrm{d}t} p_{\mathrm{a}}. \tag{2.37}$$

Since $\rho_a = M_a/V_a$, then

$$\frac{1}{\rho_a}\frac{d\rho_a}{dt} = \frac{1}{M_a}\frac{dM_a}{dt} - \frac{1}{V_a}\frac{dV_a}{dt}, \tag{2.38}$$

and thus, if the air mass is conserved in the solid skeleton volume then De_3'/Dt represents the unit power of the partial air pressure $p^a = \phi^a p_a$ in compressing the air volume.

It is illuminating to compare the above formulation to that presented by Houlsby [41,46], who postulated an expression for the mechanical power input of the form

$$\mathscr{P}' = \int_A \sum_{\alpha=s,w,a} \boldsymbol{\sigma}^\alpha : \boldsymbol{v} \otimes \boldsymbol{v}_\alpha \, dA + \int_V \sum_{\alpha=s,w,a} \rho^\alpha \mathbf{g} \cdot \boldsymbol{v}_\alpha \, dV. \tag{2.39}$$

The first term represents the power input of the surface tractions, whereas the second term represents the power input of the gravity forces. This expression for the mechanical power differs from (2.23) in that the internal body forces $\boldsymbol{h}^\alpha$ have been assumed to produce no power. Our rationale for including these forces is that even if $\sum \boldsymbol{h}^\alpha = \mathbf{0}$, $\sum \boldsymbol{h}^\alpha \cdot \boldsymbol{v}_\alpha \neq 0$ since the constituent phases are moving at different velocities and thus their individual mechanical powers do not cancel, see also [47–49].

Using the Gauss theorem on (2.39) and subtracting $D\mathscr{K}/Dt$ given by (2.21), the material time derivative of the internal energy, ignoring the mechanical power of the forces $\boldsymbol{h}^\alpha$, becomes

$$\frac{D\mathscr{I}'}{Dt} = \mathscr{P}' - \frac{D\mathscr{K}}{Dt} = \int_V \sum_{\alpha=s,w,a} (\boldsymbol{\sigma}^\alpha : \boldsymbol{l}_\alpha - \boldsymbol{h}^\alpha \cdot \boldsymbol{v}_\alpha) \, dV. \tag{2.40}$$

The above expression coincides with (2.24) only for the special case where $\boldsymbol{v}_\alpha = \boldsymbol{v}$, i.e., when the three constituent phases move at the same velocity. If we followed the developments of Section 4 step by step, the end results would be the same except for the first term De_1'/Dt which would now contain the mechanical power of the forces $\boldsymbol{h}^\alpha$.

We note that (2.26) is perfectly consistent with Eq. (6) of Biot [50], who stated that for isothermal deformations the power done on a mixture is equal to the power done by the total stresses in deforming the solid skeleton volume plus the power done by the pressure function to inject a fluid mass into the element, i.e.,

$$\frac{De}{Dt} = \boldsymbol{\sigma} : \dot{\boldsymbol{\epsilon}} + \psi \dot{m}, \tag{2.41}$$

where $\dot{\boldsymbol{\epsilon}}$ is the small strain rate computed from the motion of the solid matrix, ψ is the 'pressure function,' and m is the fluid mass injected in the soil element. In the finite deformation regime, $\dot{\boldsymbol{\epsilon}}$ generalizes to the velocity gradient $\boldsymbol{l}$, whereas the second term in (2.41) evidently has the same meaning as the term $\sum_{\alpha=w,a} \boldsymbol{\sigma}^\alpha : \tilde{\boldsymbol{l}}_\alpha$ in (2.26).

2.4. The second law of thermodynamics—reduced dissipation inequality

We denote by η the total entropy density per unit current volume of the mixture. Without loss of generality we shall assume in the following that there is no heat source and there is no heat flux in the system. The Clausius-Duhem inequality then reads

$$\frac{D}{Dt}\int_V \eta \, dV \geqslant 0 \Rightarrow \frac{D\eta}{Dt} \geqslant 0, \tag{2.42}$$

for any arbitrary current volume V.

Next, we define free energy density Ψ per unit current volume of the mixture by $\Psi = e - T\eta$, where T is the absolute temperature. For isothermal processes the time derivative of Ψ takes the form

$$\frac{D\Psi}{Dt} = \frac{De}{Dt} - T\frac{D\eta}{Dt}. \tag{2.43}$$

Assuming now that the free energy function Ψ is representative of the total mixture and that it is associated with a material point attached to the solid matrix [31], then $\mathrm{D}\Psi/\mathrm{D}t = \mathrm{d}\Psi/\mathrm{d}t \equiv \dot{\Psi}$, where the symbol $\dot{(\,)}$ denotes a material time derivative following the solid phase motion. Since $T > 0$, we obtain the inequality

$$\mathscr{E} := T\frac{\mathrm{D}\eta}{\mathrm{D}t} = \frac{\mathrm{D}e}{\mathrm{D}t} - \dot{\Psi} = \sum_{\alpha=\mathrm{s,w,a}} \boldsymbol{\sigma}^{\alpha} : \boldsymbol{d}_{\alpha} - \dot{\Psi} \geqslant 0, \tag{2.44}$$

where use is made of (2.25) for the internal mechanical strain power.

The functional form for Ψ reflects the multiphase nature of the problem at hand and depends on the specific form of the terms comprising the derivative $\mathrm{D}e/\mathrm{D}t$. Without much loss of generality we present in the following the dissipation inequality assuming infinitesimal solid matrix deformation; the case of finite deformation can be developed following very similar lines using appropriate measures of deformation (see [43]), and will be discussed upon in a future publication. Using the effective stress concept of the previous section, the dissipation inequality in the infinitesimal regime rewrites

$$\mathscr{E} = \boldsymbol{\sigma}' : \dot{\boldsymbol{\epsilon}} + \sum_{\alpha=\mathrm{w,a}} \left[\frac{1}{\rho_{\alpha}}\tilde{\boldsymbol{v}}_{\alpha} \cdot \mathrm{grad}(\rho^{\alpha})\right] p_{\alpha} - ns\dot{S}_r + \sum_{\alpha=\mathrm{w,a}} (\dot{\vartheta}^{\alpha} + \psi^{\alpha}\dot{\vartheta}^{\mathrm{s}}) p_{\alpha} - \dot{\Psi} \geqslant 0, \tag{2.45}$$

where $\dot{\boldsymbol{\epsilon}}$ is the infinitesimal strain rate tensor for the solid matrix, $\boldsymbol{\sigma}'$ is the usual constitutive effective stress tensor defined in the previous section, and $\dot{\vartheta}^{\alpha} = \phi^{\alpha}\dot{p}_{\alpha}/K_{\alpha}$ for α = s, w, a.

Assuming $\dot{\boldsymbol{\epsilon}} = \dot{\boldsymbol{\epsilon}}^{\mathrm{e}} + \dot{\boldsymbol{\epsilon}}^{\mathrm{p}}$, where $\dot{\boldsymbol{\epsilon}}^{\mathrm{e}}$ and $\dot{\boldsymbol{\epsilon}}^{\mathrm{p}}$ are the elastic and inelastic components of $\boldsymbol{\epsilon}$, respectively; and, similarly, $\dot{\vartheta}^{\alpha} = \dot{\vartheta}^{\alpha,\mathrm{e}} + \dot{\vartheta}^{\alpha,\mathrm{p}}$, we can now take a free energy function of the form

$$\Psi = \Psi(\boldsymbol{\epsilon}^{\mathrm{e}}, \tilde{\boldsymbol{u}}_{\mathrm{w}}, \tilde{\boldsymbol{u}}_{\mathrm{a}}, \vartheta^{\mathrm{s,e}}, \vartheta^{\mathrm{w,e}}, \vartheta^{\mathrm{a,e}}, \boldsymbol{\xi}), \tag{2.46}$$

where $\tilde{\boldsymbol{u}}_{\alpha}$ is defined such that $\dot{\tilde{\boldsymbol{u}}}_{\alpha} \equiv \tilde{\boldsymbol{v}}_{\alpha}$ for $\alpha = w, a$; and $\boldsymbol{\xi}$ represents the usual vector of plastic internal variables. Taking the time derivative gives

$$\dot{\Psi} = \frac{\partial \Psi}{\partial \boldsymbol{\epsilon}^{\mathrm{e}}} : \dot{\boldsymbol{\epsilon}}^{\mathrm{e}} + \sum_{\alpha=\mathrm{w,a}} \frac{\partial \Psi}{\partial \tilde{\boldsymbol{u}}_{\alpha}} \cdot \tilde{\boldsymbol{v}}_{\alpha} + \sum_{\alpha=\mathrm{s,w,a}} \frac{\partial \Psi}{\partial \vartheta^{\alpha,\mathrm{e}}} \dot{\vartheta}^{\alpha,\mathrm{e}} + \frac{\partial \Psi}{\partial \boldsymbol{\xi}} \cdot \dot{\boldsymbol{\xi}}. \tag{2.47}$$

Substituting into (2.45) gives

$$\begin{aligned} \mathscr{E} = {} & \left(\boldsymbol{\sigma}' - \frac{\partial \Psi}{\partial \boldsymbol{\epsilon}^{\mathrm{e}}}\right) : \dot{\boldsymbol{\epsilon}}^{\mathrm{e}} + \sum_{\alpha=\mathrm{w,a}} \left(g_{\alpha} - \frac{\partial \Psi}{\partial \tilde{\boldsymbol{u}}_{\alpha}}\right) \cdot \tilde{\boldsymbol{v}}_{\alpha} + \sum_{\alpha=\mathrm{w,a}} \left(p_{\alpha} - \frac{\partial \Psi}{\partial \vartheta^{\alpha,\mathrm{e}}}\right) \dot{\vartheta}^{\alpha,\mathrm{e}} \\ & + \left(\overline{p} - \frac{\partial \Psi}{\partial \vartheta^{\mathrm{s,e}}}\right) \dot{\vartheta}^{\mathrm{s,e}} + \boldsymbol{\sigma}' : \dot{\boldsymbol{\epsilon}}^{\mathrm{p}} - ns\dot{S}_r + \sum_{\alpha=\mathrm{w,a}} p_{\alpha}\dot{\vartheta}^{\alpha,\mathrm{p}} + \overline{p}\dot{\vartheta}^{\mathrm{s,p}} + \boldsymbol{q} \cdot \dot{\boldsymbol{\xi}} \geqslant 0, \end{aligned} \tag{2.48}$$

where $g_{\alpha} = p_{\alpha}\mathrm{grad}(\rho^{\alpha})/\rho_{\alpha}$ is the Gibbs potential for fluid α per unit current volume of the mixture (cf. [31]), and $\boldsymbol{q} = -\partial\Psi/\partial\boldsymbol{\xi}$. For arbitrary $\dot{\boldsymbol{\epsilon}}^{\mathrm{e}}$, $\tilde{\boldsymbol{v}}_{\alpha}$, and $\dot{\vartheta}^{\alpha,\mathrm{e}}$, standard argument leads to the constitutive equations

$$\boldsymbol{\sigma}' = \frac{\partial \Psi}{\partial \boldsymbol{\epsilon}^{\mathrm{e}}}, \quad g_{\alpha} = \left.\frac{\partial \Psi}{\partial \tilde{\boldsymbol{u}}_{\alpha}}\right|_{\alpha=\mathrm{w,a}}, \quad p_{\alpha} = \left.\frac{\partial \Psi}{\partial \vartheta^{\alpha,\mathrm{e}}}\right|_{\alpha=\mathrm{w,a}}, \quad \overline{p} = \frac{\partial \Psi}{\partial \vartheta^{\mathrm{s,e}}}. \tag{2.49}$$

Implied in the first constitutive equation above is an elastic functional relation between the effective constitutive stress tensor $\boldsymbol{\sigma}'$ and the solid matrix elastic strain tensor ϵ^{e}. Note that the constitutive equation for $\overline{p}$ is not a redundant equation since it is a function not only of p_{w} and p_{a} but also of the degree of saturation S_r. Substituting back into (2.49) leads to the reduced dissipation inequality

$$\mathscr{E} = \boldsymbol{\sigma}' : \dot{\boldsymbol{\epsilon}}^{\mathrm{p}} - ns\dot{S}_r + \sum_{\alpha=\mathrm{w,a}} p_{\alpha}\dot{\vartheta}^{\alpha,\mathrm{p}} + \overline{p}\dot{\vartheta}^{\mathrm{s,p}} + \boldsymbol{q} \cdot \dot{\boldsymbol{\xi}} \geqslant 0. \tag{2.50}$$

Except for the terms associated with the compressibilities of the three phases and the additional term $-ns\dot{S}_r$ arising from partial saturation (which vanishes in the limit of full saturation), the above reduced dissipation inequality is essentially the same as that derived for the fully saturated case [43].

3. Constitutive formulation and shear band analysis

With reference to the developments of the previous section, we herein present: (a) a constitutive framework for three-phase partially saturated media, and (b) a framework for shear band analyses at both locally drained and locally undrained conditions. In order to limit the scope of this paper, we shall follow the developments of Section 2.4 and assume that the deformation of the solid matrix is infinitesimal. As usual, the operator $(\cdot)$ denotes a material time derivative following the solid phase motion.

3.1. Maximum plastic dissipation; convexity of the yield function

The principle of maximum plastic dissipation, often credited to von Mises (see [51,52]), states that, for any stress state defined by the set $(\boldsymbol{\sigma}', s, p_w, p_a, \overline{p}, \boldsymbol{q})$, and for given $(\boldsymbol{\epsilon}^p, S_r, \vartheta^{w,p}, \vartheta^{a,p}, \vartheta^{s,p}, \boldsymbol{\xi})$, the dissipation function attains its maximum at the actual state. With reference to the reduced dissipation inequality (2.50), we have

$$\left(\boldsymbol{\sigma}' - \overset{\triangledown}{\boldsymbol{\sigma}'}\right) : \dot{\boldsymbol{\epsilon}}^p - n\left(s - \overset{\triangledown}{s}\right)\dot{S}_r + \sum_{\alpha=w,a}\left(p_\alpha - \overset{\triangledown}{p}_\alpha\right)\dot{\vartheta}^{\alpha,p} + \left(\overline{p} - \overset{\triangledown}{\overline{p}}\right)\dot{\vartheta}^{s,p} + \left(\boldsymbol{q} - \overset{\triangledown}{\boldsymbol{q}}\right)\cdot\dot{\boldsymbol{\xi}} \geqslant 0, \tag{3.1}$$

for all $\left(\overset{\triangledown}{\boldsymbol{\sigma}'}, \overset{\triangledown}{s}, \overset{\triangledown}{p}_w, \overset{\triangledown}{p}_a, \overset{\triangledown}{\overline{p}}, \overset{\triangledown}{\boldsymbol{q}}\right)$ in the admissible set **E**.

Classical plasticity theory requires a yield function representing the boundary of the elastic region. Let $F(\boldsymbol{\sigma}', s, p_w, p_a, \overline{p}, \boldsymbol{q}) = 0$ be such a yield function for the problem at hand. Note that the arguments of F are motivated by classical thermodynamics as demonstrated by the developments of the previous section. As noted in [52] maximum plastic dissipation implies the following:

(a) associativity of the flow rule in stress space,

$$\dot{\boldsymbol{\epsilon}}^p = \dot{\lambda}\frac{\partial F}{\partial \boldsymbol{\sigma}'}, \quad -\dot{S}_r = \dot{\lambda}\frac{\partial F}{\partial s}, \quad \dot{\vartheta}^{\alpha,p} = \dot{\lambda}\left.\frac{\partial F}{\partial p_\alpha}\right|_{\alpha=w,a}, \quad \dot{\vartheta}^{s,p} = \dot{\lambda}\frac{\partial F}{\partial \overline{p}}, \tag{3.2}$$

(b) associativity of the hardening in the sense

$$\dot{\boldsymbol{\xi}} = \dot{\lambda}\frac{\partial F}{\partial \boldsymbol{q}}, \quad \text{where} \quad \boldsymbol{q} = -\frac{\partial \Psi}{\partial \boldsymbol{\xi}}, \tag{3.3}$$

(c) loading/unloading conditions in Kuhn–Tucker form

$$\dot{\lambda} \geqslant 0, \quad F \leqslant 0, \quad \dot{\lambda}F = 0, \tag{3.4}$$

and, finally,

(d) convexity of the yield function F.

Implied above is that the yield function F may depend on s, p_w, and p_a, even if these three variables are not mutually independent. Obviously, one can construct more elaborate delineations of F, say,

$$F(\boldsymbol{\sigma}', s, p_w, p_a, \overline{p}, \boldsymbol{q}) = F_1(\boldsymbol{\sigma}', s, \boldsymbol{q}_1) + F_2(p_w, p_a, \overline{p}, \boldsymbol{q}_2) = 0, \tag{3.5}$$

where $\boldsymbol{q}_1 \cup \boldsymbol{q}_2 = \boldsymbol{q}$, or even 'break down' F_2 further to reflect yield conditions for the individual phases. In this case, requiring that both F_1 and F_2 vanish results in two yield functions, two sets of Kuhn–Tucker

loading/unloading conditions, two non-negative plastic multipliers $\dot{\lambda}_1$ and $\dot{\lambda}_2$, etc. However, this elaborate treatment is deemed unnecessary at this point since current limitations in experimental capabilities already inhibit a precise characterization of the plastic evolution in the solid matrix, let alone the plasticities in the individual constituent phases. If we drop the function F_2 altogether, then p_w and p_a enter into the expression for the yield function F only through the suction stress s, and thus $\vartheta^{\alpha,p} \equiv 0$ for $\alpha = s, w, a$, which implies that the individual constituent phases are assumed to behave elastically. In fact, in the following developments we shall assume further that the solid phase is incompressible, which is typical for soil grains (relative to the water and air phases). Thus, the expression for the maximum plastic dissipation reduces to

$$\left(\boldsymbol{\sigma}' - \overset{\nabla}{\boldsymbol{\sigma}'}\right) : \dot{\boldsymbol{\epsilon}}^{\mathrm{p}} - n\left(s - \overset{\nabla}{s}\right)\dot{S}_r + \left(\boldsymbol{q} - \overset{\nabla}{\boldsymbol{q}}\right) \cdot \dot{\boldsymbol{\xi}} \geqslant 0. \tag{3.6}$$

Thus, a yield function of the form $F(\boldsymbol{\sigma}', s, \boldsymbol{q}) = 0$ would guarantee maximum dissipation if

$$\dot{\boldsymbol{\epsilon}}^{\mathrm{p}} = \dot{\lambda}\frac{\partial F}{\partial \boldsymbol{\sigma}'}, \quad -\dot{S}_r = \dot{\lambda}\frac{\partial F}{\partial s}, \quad \dot{\boldsymbol{\xi}} = \dot{\lambda}\frac{\partial F}{\partial \boldsymbol{q}}. \tag{3.7}$$

Note again that the inclusion of s in the arguments of F is motivated by thermodynamic considerations.

In reality, the developments shown above are only useful theoretically but generally cannot reproduce observed soil behavior since soils do not obey any of the normality rule in the sense of (3.7). In the following section we describe a constitutive framework, based on Cam-Clay plasticity theory, that more accurately captures the observed mechanical behavior of partially saturated soils. This model does not satisfy any of the three equations in (3.7), and some authors have even noted that the resulting yield function is non-convex [53,54]. We show in Section 4.4 that this lack of convexity of the yield function does not engender any numerical problem with regard to the implementation of the widely used return mapping algorithm of computational plasticity.

3.2. Constitutive framework

We recall from the previous section that the constitutive laws must relate: (a) the evolution of the constitutive effective stress $\boldsymbol{\sigma}'$ with imposed solid matrix deformation $\boldsymbol{\epsilon}$; (b) the degree of saturation S_r with suction stress s; (c) the intrinsic mass densities with intrinsic pressures on all three phases; and (d) the relative flow vector $\tilde{\boldsymbol{v}}_\alpha$ with intrinsic pressure p_α for the water and air phases. We elaborate each aspect of these constitutive relations in the following.

(1) *Constitutive model for solid matrix*. For the solid matrix we assume an elastoplastic behavior described by a yield function of the form $F = F(\boldsymbol{\sigma}', s, p_c) = 0$, where the scalar variable p_c now takes the role of $\boldsymbol{q}$ in the argument of F representing a stress-like plastic internal variable *at zero suction*. We then assume a rate expression for the effective constitutive stress $\boldsymbol{\sigma}'$ of the form

$$\dot{\boldsymbol{\sigma}}' = \boldsymbol{c}^{\mathrm{e}} : (\dot{\boldsymbol{\epsilon}} - \dot{\lambda}\boldsymbol{g}), \quad \boldsymbol{g} = \frac{\partial G}{\partial \boldsymbol{\sigma}'}, \tag{3.8}$$

where $\boldsymbol{c}^{\mathrm{e}} = \partial^2\Psi/\partial\boldsymbol{\epsilon}^{\mathrm{e}}\partial\boldsymbol{\epsilon}^{\mathrm{e}}$ is the Hessian of the free energy function Ψ, $\dot{\boldsymbol{\epsilon}}$ is the total strain rate tensor, G is the plastic potential function, and $\dot{\lambda}$ is a non-negative plastic multiplier satisfying the usual Kuhn–Tucker conditions

$$\dot{\lambda} \geqslant 0, \quad F(\boldsymbol{\sigma}', s, p_c) \leqslant 0, \quad \dot{\lambda}F(\boldsymbol{\sigma}', s, p_c) = 0. \tag{3.9}$$

Next, we consider a phenomenological hardening law of the form

$$\dot{p}_c = \dot{\lambda}h(\boldsymbol{\sigma}', p_c), \tag{3.10}$$

where h is a scalar-valued function. Many constitutive hardening laws for geomaterials can be cast in the above form. For Cam-Clay-type models $\dot{p}_c$ usually varies with $\dot{\lambda}$ through the volumetric component of the plastic strain, $\dot{\epsilon}_v^p = \mathrm{tr}(\dot{\boldsymbol{\epsilon}}^p) = \dot{\lambda}\mathrm{tr}(\boldsymbol{g})$. The quantity h is generally a function of $\boldsymbol{\sigma}'$ and even p_c itself. The consistency condition can be written as

$$\dot{F} = \boldsymbol{f} : \dot{\boldsymbol{\sigma}}' + \varphi\dot{s} - H\dot{\lambda} = 0, \tag{3.11}$$

where

$$\boldsymbol{f} = \frac{\partial F}{\partial \boldsymbol{\sigma}'}, \quad \varphi = \frac{\partial F}{\partial s}, \quad H = -\frac{\partial F}{\partial p_c} h(\boldsymbol{\sigma}', p_c), \tag{3.12}$$

with H being the generalized plastic modulus. For a constant s the sign of H determines the type of response: hardening if $H > 0$, softening if $H < 0$, and perfectly plastic if $H = 0$. Note that for a non-stationary s the sign of H alone does not determine whether the material is hardening, softening, or exhibiting a perfectly plastic response.

Solving for the plastic multiplier gives

$$\dot{\lambda} = \frac{1}{\chi}(\boldsymbol{f} : \boldsymbol{c}^e : \dot{\boldsymbol{\epsilon}} + \varphi\dot{s}), \quad \chi = \boldsymbol{f} : \boldsymbol{c}^e : \boldsymbol{g} + H. \tag{3.13}$$

Since $\dot{\lambda} > 0$ and $\chi > 0$ for a plastic process (the latter inequality is required for an acceptable material response, see [55]), we must have

$$\boldsymbol{f} : \boldsymbol{c}^e : \dot{\boldsymbol{\epsilon}} + \varphi\dot{s} > 0. \tag{3.14}$$

Note that the sign of the scalar product $\boldsymbol{f} : \boldsymbol{c}^e : \dot{\boldsymbol{\epsilon}}$ alone does not determine whether the material is yielding plastically or unloading elastically; the variation of s also must be considered. With the above form for $\dot{\lambda}$, the rate constitutive equation now becomes

$$\dot{\boldsymbol{\sigma}}' = \boldsymbol{c}^{ep} : \dot{\boldsymbol{\epsilon}} - \frac{1}{\chi}(\boldsymbol{c}^e : \boldsymbol{g})\varphi\dot{s}, \tag{3.15}$$

where

$$\boldsymbol{c}^{ep} = \boldsymbol{c}^e - \frac{1}{\chi}\boldsymbol{c}^e : \boldsymbol{g} \otimes \boldsymbol{f} : \boldsymbol{c}^e \tag{3.16}$$

is the elastoplastic constitutive tensor. If $\dot{s} = 0$ we recover the classical elastoplastic constitutive relations.

(2) *Degree of saturation–matrix suction relation*. A number of phenomenological relationships exist relating the matrix suction s to the degree of saturation S_r (e.g., the Brooks–Corey [56] and van Genuchten [57] relations). For isothermal loading we consider a constitutive relation of the form

$$S_r = S_r(s), \tag{3.17}$$

This law may be influenced by the so-called air entry value (or bubbling pressure), which is the characteristic pressure required before the air enters the pores. The material time derivatives, again following the motion of the solid matrix, are given by

$$\dot{S}_r = S_r'(s)(\dot{p}_a - \dot{p}_w). \tag{3.18}$$

The slope $S_r'(s)$ determines the rate of change of S_r as a function of the rate of change of s.

(3) *Intrinsic mass density–intrinsic pressure relations*. The intrinsic mass densities and intrinsic pressures on all three phases are related by the bulk moduli of the corresponding constituent phases, scaled by the intrinsic mass densities, see (2.9). The bulk moduli K_s and K_w are available from handbooks of material properties [58], and K_s for solids may be considered infinite for practical purposes. The bulk modulus K_a

of the air phase typically depends on the temperature; however, for isothermal deformations Boyle–Mariotte's law may be assumed to hold [59], i.e., $p_a V_a = p_a M_a/\rho_a$ = constant, and thus we have

$$\dot{(p_a M_a/\rho_a)} = 0. \tag{3.19}$$

Expanding the derivative, noting that $\dot{p}_a = p'_a(\rho_a)\dot{\rho}_a$ for barotropic flows, and using the definition of the bulk modulus for the air phase, we get

$$\frac{\rho_a p_a}{M_a}\dot{M}_a + (K_a - p_a)\dot{\rho}_a = 0, \tag{3.20}$$

where $\dot{M}_a$ is the net change in the total air mass contained in the volume V of the moving solid matrix. If the mass M_a is conserved in the volume V then $\dot{M}_a = 0$ and we get $K_a = p_a$, i.e., the bulk modulus K_a is equal to the (absolute) intrinsic air pressure p_a.

(4) *Diffusion constitutive relations*. We seek constitutive laws relating the relative flow vector $\tilde{\boldsymbol{v}}^\alpha = \phi^\alpha \tilde{\boldsymbol{v}}_\alpha$ to the intrinsic pressure p_α for α = w, a. Alternatively, we can relate $\tilde{\boldsymbol{v}}_\alpha = \boldsymbol{v}_\alpha - \boldsymbol{v}$ to the internal body force $\boldsymbol{h}^\alpha$ via the constitutive equations

$$\boldsymbol{h}^\alpha = -\boldsymbol{\xi}^\alpha \cdot \tilde{\boldsymbol{v}}_\alpha, \tag{3.21}$$

where

$$\boldsymbol{\xi}^\alpha = (\phi^\alpha)^2 \left(\frac{\boldsymbol{k}^\alpha}{\mu_\alpha}\right)^{-1} \tag{3.22}$$

are symmetric positive-definite second-order tensors. The term $\boldsymbol{k}^\alpha$ (with dimension L^2, or Darcy, as used in the oil industry) is the tensor of specific or intrinsic permeabilities of the α pore, and μ_α is the viscosity of the α permeant. However, balance of momentum for the two fluid phases gives

$$\boldsymbol{h}^\alpha = \operatorname{grad}(\phi^\alpha p_\alpha) + \rho^\alpha(\boldsymbol{a}_\alpha - \mathbf{g}), \tag{3.23}$$

where $\boldsymbol{a}_\alpha = \dot{\boldsymbol{v}}_\alpha$. Thus, combining (3.21) and (3.23) gives the desired diffusion constitutive relations (see also [60,61]).

3.3. Shear band analyses

The model described above is suitable for strain localization analysis into tabular deformation bands. Under conditions of locally drained and locally undrained deformations, criteria for the emergence of a tabular deformation band may be formulated. To capture a tabular deformation band, and following the notation of [62], we define a velocity field by the ramp-like relation

$$\boldsymbol{v} = \begin{cases} \bar{\boldsymbol{v}} & \text{if } \eta \leqslant 0, \\ \bar{\boldsymbol{v}} + \eta[\![\boldsymbol{v}]\!]/h & \text{if } 0 \leqslant \eta \leqslant h, \\ \bar{\boldsymbol{v}} + [\![\boldsymbol{v}]\!] & \text{if } \eta \geqslant h, \end{cases} \tag{3.24}$$

where $\bar{\boldsymbol{v}}$ is a continuous velocity field and $[\![\boldsymbol{v}]\!]$ represents the relative velocity of the opposite faces of the band. Assuming $[\![\boldsymbol{v}]\!]$ is uniform over $\hat{\mathscr{S}}$, the corresponding velocity gradient fields outside and inside the band take the form

$$\boldsymbol{l} = \begin{cases} \nabla\bar{\boldsymbol{v}} & \text{in } \Omega \setminus \bar{\mathscr{D}}, \\ \nabla\bar{\boldsymbol{v}} + ([\![\boldsymbol{v}]\!] \otimes \boldsymbol{n})/h & \text{in } \mathscr{D} \end{cases} \tag{3.25}$$

where $\mathscr{D} = \mathscr{S} \times (0, h)$ is the open band domain, $\bar{\mathscr{D}}$ is the closure of $\mathscr{D}$, and $\boldsymbol{n}$ is the unit normal vector to the band (since h is assumed small, $\boldsymbol{n}$ may be taken as normal to either $\mathscr{S}$ or $\hat{\mathscr{S}}$). We note that the orientation of

$\boldsymbol{n}$ is perfectly symmetric in the sense that it may be directed either outward or inward to the band. The velocity gradient is thus discontinuous across the band, and upon evaluating just inside and just outside the surface of discontinuity we obtain the relations

$$\boldsymbol{l}^1 = \boldsymbol{l}^0 + \frac{1}{h}[\![\boldsymbol{v}]\!] \otimes \boldsymbol{n} \Longleftrightarrow \dot{\boldsymbol{\epsilon}}^1 = \dot{\boldsymbol{\epsilon}}^0 + \frac{1}{h}\mathrm{sym}([\![\boldsymbol{v}]\!] \otimes \boldsymbol{n}), \tag{3.26}$$

where $\dot{\boldsymbol{\epsilon}}^1 = \mathrm{sym}(\boldsymbol{l}^1)$ and $\dot{\boldsymbol{\epsilon}}^0 = \mathrm{sym}(\boldsymbol{l}^0)$. Throughout this paper we will use the superscript symbols "1" and "0" to refer to points on $\mathscr{S}$ interpreted to lie just inside and just outside this surface, respectively.

From (2.31) the total Cauchy stress rate tensor can be obtained from the chain rule as

$$\dot{\boldsymbol{\sigma}} = \dot{\boldsymbol{\sigma}}' - \dot{\bar{p}}\mathbf{1}, \quad \dot{\bar{p}} = \overline{S}_r \dot{p}_{\mathrm{w}} + (1 - \overline{S}_r)\dot{p}_{\mathrm{a}}, \quad \overline{S}_r := S_r + S_r'(s)s, \tag{3.27}$$

where we have used (3.18) for $\dot{S}_r(s)$. We recall the effective constitutive stress rate $\dot{\boldsymbol{\sigma}}'$ to have the form

$$\dot{\boldsymbol{\sigma}}' = \boldsymbol{c}^{\mathrm{ep}} : \dot{\boldsymbol{\epsilon}} - \frac{\varphi}{\chi}(\boldsymbol{c}^{\mathrm{e}} : \boldsymbol{g})\dot{s}, \quad \dot{s} = \dot{p}_{\mathrm{a}} - \dot{p}_{\mathrm{w}}, \tag{3.28}$$

where $\dot{\boldsymbol{\epsilon}}$ is the strain rate in the solid matrix and $\dot{s}$ is the matrix suction rate.

We first consider the case of fully drained condition. In this case the Cauchy stress rate just outside the band is given by

$$\dot{\boldsymbol{\sigma}}^0 = \boldsymbol{c}^{\mathrm{ep}} : \dot{\boldsymbol{\epsilon}}^0 - \left[\frac{\varphi}{\chi}\boldsymbol{c}^{\mathrm{e}} : \boldsymbol{g} + (1 - \overline{S}_r)\mathbf{1}\right]\dot{p}_{\mathrm{a}}^0 + \left(\frac{\varphi}{\chi}\boldsymbol{c}^{\mathrm{e}} : \boldsymbol{g} - \overline{S}_r\mathbf{1}\right)\dot{p}_{\mathrm{w}}^0, \tag{3.29}$$

whereas the Cauchy stress rate just inside is

$$\dot{\boldsymbol{\sigma}}^1 = \boldsymbol{c}^{\mathrm{ep}} : \dot{\boldsymbol{\epsilon}}^1 - \left[\frac{\varphi}{\chi}\boldsymbol{c}^{\mathrm{e}} : \boldsymbol{g} + (1 - \overline{S}_r)\mathbf{1}\right]\dot{p}_{\mathrm{a}}^1 + \left(\frac{\varphi}{\chi}\boldsymbol{c}^{\mathrm{e}} : \boldsymbol{g} - \overline{S}_r\mathbf{1}\right)\dot{p}_{\mathrm{w}}^1. \tag{3.30}$$

By fully drained condition we mean that the pore pressures inside and outside the band are continuous, i.e., $\dot{p}_{\mathrm{a}}^0 = \dot{p}_{\mathrm{a}}^1$, and $\dot{p}_{\mathrm{w}}^0 = \dot{p}_{\mathrm{w}}^1$. Continuity of the incremental traction vector then requires that

$$\boldsymbol{n} \cdot \dot{\boldsymbol{\sigma}}^0 = \boldsymbol{n} \cdot \dot{\boldsymbol{\sigma}}^1. \tag{3.31}$$

This results in the usual localization condition

$$\boldsymbol{A} \cdot \boldsymbol{m} = \mathbf{0}, \quad \boldsymbol{A} = \boldsymbol{n} \cdot \boldsymbol{c}^{\mathrm{ep}} \cdot \boldsymbol{n}. \tag{3.32}$$

In the above, $\boldsymbol{A}$ is the elastoplastic acoustic tensor calculated from the elastoplastic constitutive operator $\boldsymbol{c}^{\mathrm{ep}}$ for the underlying drained solid, and $\boldsymbol{m}$ is the unit vector in the direction of the jump velocity vector $[\![\boldsymbol{v}]\!]$. Observe that the effect of the matrix suction enters only through the elastoplastic constitutive tensor $\boldsymbol{c}^{\mathrm{ep}}$ of the underlying drained solid.

Next we consider the problem of locally undrained deformation. By fully undrained condition we mean that $\boldsymbol{v}_{\mathrm{a}} = \boldsymbol{v}_{\mathrm{w}} = \boldsymbol{v}$, i.e., all three phases move as one material and thus the masses of the pore air and pore water phases are conserved in the motion of the solid matrix. This means that it is possible to calculate the pore air and pore water pressures from the motion of the solid matrix alone, and thus their bulk stiffnesses can be statically condensed with the elastoplastic constitutive tensor $\boldsymbol{c}^{\mathrm{ep}}$ for the drained solid to arrive at a total undrained elastoplastic constitutive tensor for the entire three-phase mixture.

Without loss of generality, we assume in the following that the solid grains are incompressible relative to the water and air phases. This is a reasonable assumption in a majority of cases; if we insist to include the solid grain compressibility in the formulation, the developments presented below require only simple modifications. With this assumption, we then rewrite the balance of mass for the solid phase, (2.10a), as

$$\dot{\phi}^{\mathrm{s}} = -\phi^{\mathrm{s}}\mathrm{div}(\boldsymbol{v}), \tag{3.33}$$

where a simple overdot has been used since the three phases move together as one body and thus there is no ambiguity as to what motion we follow. From the relations

$$\phi^{\mathrm{w}} = (1-\phi^{\mathrm{s}})\psi^{\mathrm{w}}, \quad \phi^{\mathrm{a}} = (1-\phi^{\mathrm{s}})\psi^{\mathrm{a}}, \quad \psi^{\mathrm{w}} = S_r, \quad \psi^{\mathrm{a}} = 1 - S_r, \tag{3.34}$$

we get

$$\dot{\phi}^{\mathrm{w}} = (1-\phi^{\mathrm{s}})\dot{\psi}^{\mathrm{w}} - \psi^{\mathrm{w}}\dot{\phi}^{\mathrm{s}}, \quad \dot{\phi}^{\mathrm{a}} = (1-\phi^{\mathrm{s}})\dot{\psi}^{\mathrm{a}} - \psi^{\mathrm{a}}\dot{\phi}^{\mathrm{s}}, \tag{3.35}$$

where

$$\dot{\psi}^{\mathrm{w}} = -\dot{\psi}^{\mathrm{a}} = \dot{S}_r = S_r'(s)(\dot{p}_{\mathrm{a}} - \dot{p}_{\mathrm{w}}). \tag{3.36}$$

The last equation emanates from the assumed constitutive relation between the degree of saturation and the matrix suction.

We now use (3.33), along with (3.35) and (3.36), to rewrite the balance of mass for the water phase, (2.10b) with $\boldsymbol{w}^{\mathrm{w}} = \boldsymbol{0}$, as

$$S_r'(s)(1-\phi^{\mathrm{s}})\dot{p}_{\mathrm{a}} + \left[\frac{\phi^{\mathrm{w}}}{K_{\mathrm{w}}} - S_r'(s)(1-\phi^{\mathrm{s}})\right]\dot{p}_{\mathrm{w}} = -\psi^{\mathrm{w}}\mathrm{div}(\boldsymbol{v}), \tag{3.37}$$

and the balance of mass for the air phase, (2.10c) with $\boldsymbol{w}^{\mathrm{a}} = \boldsymbol{0}$, as

$$\left[\frac{\phi^{\mathrm{a}}}{K_{\mathrm{a}}} - S_r'(s)(1-\phi^{\mathrm{s}})\right]\dot{p}_{\mathrm{a}} + S_r'(s)(1-\phi^{\mathrm{s}})\dot{p}_{\mathrm{w}} = -\psi^{\mathrm{a}}\mathrm{div}(\boldsymbol{v}). \tag{3.38}$$

We see that the expressions for $\dot{p}_{\mathrm{a}}$ and $\dot{p}_{\mathrm{w}}$ may be uncoupled when $S_r'(s) = 0$, which occurs when the solid matrix is either nearly wet or nearly dry (see Section 5). The partially saturated case requires a simultaneous solution of these equations in general, which gives

$$\dot{p}_{\mathrm{a}} = -\overline{\lambda}^{\mathrm{a}}\mathrm{div}(\boldsymbol{v}), \quad \dot{p}_{\mathrm{w}} = -\overline{\lambda}^{\mathrm{w}}\mathrm{div}(\boldsymbol{v}), \tag{3.39}$$

where

$$\overline{\lambda}^{\mathrm{a}} = \frac{1}{D}\left[S_r'(s)(1-\phi^{\mathrm{s}}) - \frac{\psi^{\mathrm{a}}\phi^{\mathrm{w}}}{K_{\mathrm{w}}}\right], \tag{3.40a}$$

$$\overline{\lambda}^{\mathrm{w}} = \frac{1}{D}\left[S_r'(s)(1-\phi^{\mathrm{s}}) - \frac{\psi^{\mathrm{w}}\phi^{\mathrm{a}}}{K_{\mathrm{a}}}\right], \tag{3.40b}$$

$$D = S_r'(s)(1-\phi^{\mathrm{s}})\left(\frac{\phi^{\mathrm{w}}}{K_{\mathrm{w}}} + \frac{\phi^{\mathrm{a}}}{K_{\mathrm{a}}}\right) - \frac{\phi^{\mathrm{a}}\phi^{\mathrm{w}}}{K_{\mathrm{a}}K_{\mathrm{w}}}. \tag{3.40c}$$

We now reformulate the elastoplastic constitutive operators for a three-phase mixture moving as one body. Noting that $\dot{s} = -(\overline{\lambda}^{\mathrm{a}} - \overline{\lambda}^{\mathrm{w}})\mathrm{div}(\boldsymbol{v})$ and $\mathrm{div}(\boldsymbol{v}) = \boldsymbol{1} : \dot{\boldsymbol{\epsilon}}$ for infinitesimal deformation, the effective constitutive stress rate $\dot{\boldsymbol{\sigma}}'$ from (3.28) reduces to the form

$$\dot{\boldsymbol{\sigma}}' = \overline{\boldsymbol{c}}^{\mathrm{ep}} : \dot{\boldsymbol{\epsilon}}, \quad \overline{\boldsymbol{c}}^{\mathrm{ep}} = \boldsymbol{c}^{\mathrm{ep}} + \frac{\varphi}{\chi}(\overline{\lambda}^{\mathrm{a}} - \overline{\lambda}^{\mathrm{w}})\boldsymbol{c}^{\mathrm{e}} : \boldsymbol{g} \otimes \boldsymbol{1}. \tag{3.41}$$

The total stress rate $\dot{\boldsymbol{\sigma}}$ from (3.27) becomes

$$\dot{\boldsymbol{\sigma}} = \tilde{\boldsymbol{c}}^{\mathrm{ep}} : \dot{\boldsymbol{\epsilon}}, \quad \tilde{\boldsymbol{c}}^{\mathrm{ep}} = \overline{\boldsymbol{c}}^{\mathrm{ep}} + \overline{\lambda}^{\mathrm{v}}\boldsymbol{1} \otimes \boldsymbol{1}, \tag{3.42}$$

where

$$\overline{\lambda}^{\mathrm{v}} = \overline{S}_r\overline{\lambda}^{\mathrm{w}} + (1-\overline{S}_r)\overline{\lambda}^{\mathrm{a}} \tag{3.43}$$

is the average bulk modulus of the void, $\overline{S}_r = S_r + S_r'(s)s$, and $\tilde{\boldsymbol{c}}^{\rm ep}$ is the undrained elastoplastic constitutive tensor of the total mixture. The modulus $\overline{\lambda}^{\rm v}$ relates the weighted pore pressure rate $\dot{\overline{p}}$ (see (2.31) and (2.34)) to the volumetric strain rate of the solid matrix, div($\boldsymbol{v}$), under a locally undrained condition, i.e.,

$$\dot{\overline{p}} = -\overline{\lambda}^{\rm v}\,\mathrm{div}(\boldsymbol{v}). \tag{3.44}$$

When the material is nearly dry $\overline{S}_r \approx 0$, which gives $\overline{\lambda}^{\rm v} \approx \overline{\lambda}^{\rm a} = K_{\rm a}/\phi^{\rm a}$. Similarly, $\overline{S} \approx 1$ when the material is nearly saturated, which gives $\overline{\lambda}^{\rm v} \approx \overline{\lambda}^{\rm w} = K_{\rm w}/\phi^{\rm w}$. This suggests a range $K_{\rm a}/(1-\phi^{\rm s}) \leqslant \overline{\lambda}^{\rm v} \leqslant K_{\rm w}/(1-\phi^{\rm s})$, where $(1-\phi^{\rm s}) \equiv n$ is the porosity of the mixture. In reality, the formulation for partially saturated medium does not allow the degree of saturation to equal zero or unity exactly, as elaborated in the next section.

The condition for the emergence of a tabular deformation band for a three-phase mixture under a locally undrained condition is as follows. Let $\dot{\boldsymbol{\sigma}}^0 = \tilde{\boldsymbol{c}}^{\rm ep} : \dot{\boldsymbol{\epsilon}}^0$ and $\dot{\boldsymbol{\sigma}}^1 = \tilde{\boldsymbol{c}}^{\rm ep} : \dot{\boldsymbol{\epsilon}}^1$, continuity of the incremental traction vector, $\boldsymbol{n}\cdot\dot{\boldsymbol{\sigma}}^0 = \boldsymbol{n}\cdot\dot{\boldsymbol{\sigma}}^1$, results in the localization condition

$$\tilde{\boldsymbol{A}}\cdot\boldsymbol{m} = \boldsymbol{0}, \quad \tilde{\boldsymbol{A}} = \boldsymbol{n}\cdot\tilde{\boldsymbol{c}}^{\rm ep}\cdot\boldsymbol{n}. \tag{3.45}$$

Note that the acoustic tensor $\tilde{\boldsymbol{A}}$ is now calculated from the total elastoplastic constitutive operator $\tilde{\boldsymbol{c}}^{\rm ep}$ for the entire mixture. Because the pore air and pore water pressures depend on the motion of the solid matrix, which in turn admits a possible discontinuity in the form of a jump in the velocity gradient field, the above undrained formulation likewise admits a possible jump in the incremental pore air and pore water pressures across the band.

4. Formulation and implementation of a constitutive model

Enhanced versions of Cam-Clay-type models have been developed over the years to capture the mechanical behavior of partially saturated soils [6–9,14,15]. These models contain the suction stress s as an additional variable, which influences the effective size of the elastic region as well as the amount of plastic deformation. In the limit of full saturation they reduce to classical Cam-Clay plasticity models. In the presentation below we describe a particular version that we have implemented using the classical return mapping algorithm of computational plasticity. To limit the scope of the presentation we shall focus only on the infinitesimal case and address finite deformation effects in a future work.

4.1. Analytical model

The first element of the model describes the non-linear elastic response. Here, we assume a free energy function of the form

$$\Psi = \Psi^{\rm e}(\boldsymbol{\epsilon}^{\rm e}) + \hat{\Psi}(\tilde{\boldsymbol{u}}_{\rm w}, \tilde{\boldsymbol{u}}_{\rm a}, \vartheta^{\rm s,e}, \vartheta^{\rm w,e}, \vartheta^{\rm a,e}, \boldsymbol{\xi}), \tag{4.1}$$

where $\Psi^{\rm e}(\boldsymbol{\epsilon}^{\rm e})$ is the stored elastic strain energy. The effective constitutive stress $\boldsymbol{\sigma}'$ may thus be expressed as

$$\boldsymbol{\sigma}' = \frac{\partial\Psi^{\rm e}}{\partial\boldsymbol{\epsilon}^{\rm e}}. \tag{4.2}$$

Specifically, we assume that $\Psi^{\rm e}$ takes the form (see [34,35] for further details)

$$\Psi^{\rm e}(\boldsymbol{\epsilon}^{\rm e}) = \tilde{\Psi}^{\rm e}(\epsilon_{\rm v}^{\rm e}) + \frac{3}{2}\mu^{\rm e}\epsilon_{\rm s}^{\rm e2}, \tag{4.3}$$

where

$$\tilde{\Psi}^{\rm e}(\epsilon_{\rm v}^{\rm e}) = -p_0\tilde{\kappa}\exp\omega, \quad \omega = -\frac{\epsilon_{\rm v}^{\rm e} - \epsilon_{\rm v0}^{\rm e}}{\tilde{\kappa}}, \quad \mu^{\rm e} = \mu_0 + \frac{\alpha}{\tilde{\kappa}}\tilde{\Psi}^{\rm e}(\epsilon_{\rm v}^{\rm e}). \tag{4.4}$$

The independent variables are the infinitesimal volumetric and deviatoric strain invariants

$$\epsilon_{\mathrm{v}}^{\mathrm{e}} = \mathrm{tr}(\boldsymbol{\epsilon}^{\mathrm{e}}), \quad \epsilon_{\mathrm{s}}^{\mathrm{e}} = \sqrt{\frac{2}{3}}\|\boldsymbol{e}^{\mathrm{e}}\|, \quad \boldsymbol{e}^{\mathrm{e}} = \boldsymbol{\epsilon}^{\mathrm{e}} - \frac{1}{3}\epsilon_{\mathrm{v}}^{\mathrm{e}}\mathbf{1}. \tag{4.5}$$

The required material parameters are the reference strain $\epsilon_{\mathrm{v0}}^{\mathrm{e}}$ and reference pressure p_0 of the elastic compression curve, and the elastic compressibility index $\tilde{\kappa}$. The above model produces pressure-dependent elastic bulk and shear moduli, in accord with an accepted soil behavioral feature. The model permits the capture of a constant elastic shear modulus $\mu^{\mathrm{e}} = \mu_0$ by setting $\alpha = 0$ in (4.4). This non-linear elasticity model is conservative in the sense that no energy is generated or lost in a closed loading cycle [63]. That Ψ^{e} has been isolated from s implies that the suction stress does not influence the elastic response, see also [6].

The second element of the formulation describes the plasticity model. Here, we first define the volumetric and deviatoric stress invariants of $\boldsymbol{\sigma}'$ as

$$p' = \frac{1}{3}\mathrm{tr}(\boldsymbol{\sigma}'), \quad q = \sqrt{\frac{3}{2}}\|\boldsymbol{s}\|, \quad \boldsymbol{s} = \boldsymbol{\sigma}' - p'\mathbf{1}. \tag{4.6}$$

Note the boldfaced symbol $\boldsymbol{s}$ for the deviatoric Cauchy stress tensor should not be confused with the light-faced symbol s for the suction stress. More specifically, we assume a two-invariant yield function of the form

$$F(\boldsymbol{\sigma}', s, p_{\mathrm{c}}) = \frac{q^2}{M^2} + (p' - p'_{\mathrm{s}})(p' - \overline{p}_{\mathrm{c}}) = 0. \tag{4.7}$$

This yield surface has the shape of an ellipsoid in principal stress space, with the hydrostatic axis as the generating axis. The parameter M is related to the internal friction angle of the material and defines the geometric axis ratio of the ellipsoid. The 'noses' of the ellipsoid on the hydrostatic axis where $q = 0$ have coordinates $p' = p'_{\mathrm{s}} \geqslant 0$ and $p' = \overline{p}_{\mathrm{c}} < 0$, see Fig. 1.

The first coordinate p'_{s} captures the apparent adhesion developed in the material resulting from the application of the matrix suction. Theoretically speaking, $p'_{\mathrm{s}} = 0$ in the effective constitutive stress formulation, but in a net stress formulation the yield surface shifts to the tension side to accommodate the suction-dependency of the critical state line [6]. To accommodate both formulations, and to show that the performance of the algorithm is not affected by the presence of this additional stress variable, we shall take the form

$$p'_{\mathrm{s}} = ks, \tag{4.8}$$

where k is a dimensionless material parameter that can be set equal to zero or greater than zero depending on the type of stress formulation.

The second coordinate $\overline{p}_{\mathrm{c}}$ is the *effective* preconsolidation stress, which is assumed to vary with the plastic volumetric strain $\epsilon_{\mathrm{v}}^{\mathrm{p}}$ and the matrix suction s. The word 'effective' is used for $\overline{p}_{\mathrm{c}}$ to suggest that the active yield

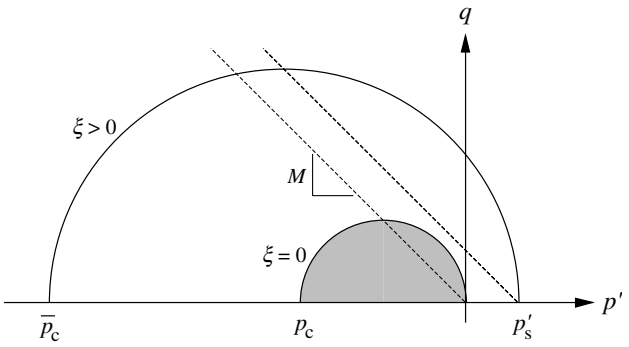

Fig. 1. Yield surface on the p'–q plane.

function can expand or shrink depending on the applied matrix suction s, even in the absence of any plastic deformation [14]. For the evolution of $\overline{p}_c$ we adopt the compressibility law proposed by Gallipoli et al. [15], a variant of the evolution law proposed by Loret and Khalili [14] based on the notion of effective stresses, except that we now use the specific volume $v = 1 + e$ (defined as the total volume of the mixture for a unit volume of the solid phase) in lieu of the void ratio e. The use of the specific volume v is consistent with the bilogarithmic compressibility law proposed by Butterfield [64], and is shown in [34] to lead to an analytical formulation amenable to implicit numerical integration. The expression for $\overline{p}_c$ is (see Eq. (10) of [15])

$$\overline{p}_c = -\exp[a(\xi)](-p_c)^{b(\xi)}, \tag{4.9}$$

where

$$a(\xi) = \frac{N[c(\xi) - 1]}{\tilde{\lambda}c(\xi) - \tilde{\kappa}}, \quad b(\xi) = \frac{\tilde{\lambda} - \tilde{\kappa}}{\tilde{\lambda}c(\xi) - \tilde{\kappa}}. \tag{4.10}$$

Note the typographical error for $a(\xi)$ in Eq. (10) of [15] where the term "$1 + N$" should read simply as "N."

The scalar dimensionless quantity $\xi \geqslant 0$ in (4.9) is called the 'bonding variable' and has a minimum value of zero in the fully saturated limit. It varies with the air void fraction $(1 - S_r)$ and a suction function $f(s)$ according to the equation

$$\xi = f(s)(1 - S_r), \quad f(s) = 1 + \frac{s/p_{atm}}{10.7 + 2.4(s/p_{atm})}, \tag{4.11}$$

where $p_{atm} = 101.3$ kPa $= 14.7$ psi is the (normalizing) atmospheric pressure. The suction function $f(s)$ is a hyperbolic approximation to the curve developed by Fisher [65] describing the meniscus-induced interparticle force between two identical spheres (see Fig. 2); as s increases this interparticle force increases, and thus the function $f(s)$ increases. The void fraction $(1 - S_r)$, on the other hand, accounts for the number of water menisci in the partially saturated mixture, reducing to zero in the perfect saturation limit. For isothermal deformations S_r may be expressed as a function of s alone, and below we adopt the relation between S_r and s proposed by van Genuchten [57] as

$$S_r = S_1 + (S_2 - S_1)\left[1 + \left(\frac{s}{s_a}\right)^n\right]^{-m}, \tag{4.12}$$

where S_1 is the residual degree of saturation below which it is no longer possible to withdraw water from the pores (which has a value somewhat greater than zero), S_2 is the maximum degree of saturation on subsequent wetting of the soil (which has a value somewhat less than unity due to trapped air bubbles), s_a is the air entry value, or bubbling pressure, and m and n are parameters to fit the experimental data. We see that for isothermal deformations within the degree of saturation range $S_1 < S_r < S_2$, ξ may be expressed in terms of s alone. Typical plots of the $S_r - s$ functions for silt and marl are shown in Fig. 3 [2,3].

The parameter $c(\xi)$ represents the ratio between the specific volume v of the virgin compression curve in the partially saturated state to the corresponding specific volume v_{sat} in the fully saturated state. That this ratio is a unique function of ξ has been demonstrated by Gallipoli and co-workers [15] to be true for various soils. Strictly, Gallipoli and co-workers showed that the ratio between the void ratio e in the partially saturated state to the corresponding void ratio e_{sat} in the fully saturated state is given by the curve

$$\frac{e}{e_{sat}} = 1 - \tilde{c}_1[1 - \exp(c_2\xi)], \tag{4.13}$$

where $\tilde{c}_1$ and c_2 are fitting parameters. Thus, the corresponding ratio of specific volumes is

$$c(\xi) := \frac{v}{v_{sat}} = \frac{1 + e}{1 + e_{sat}} = \frac{1/e_{sat} + e/e_{sat}}{1/e_{sat} + 1} = 1 - c_1[1 - \exp(c_2\xi)], \tag{4.14}$$

where $c_1 = \tilde{c}_1/(1/e_{sat} + 1)$.

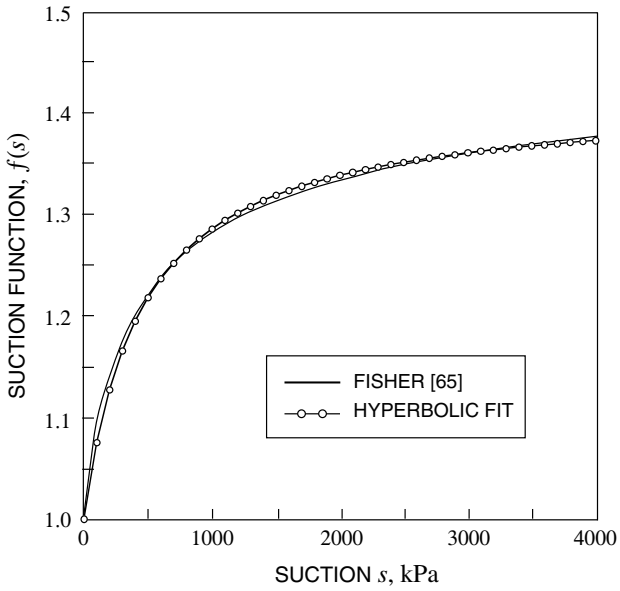

Fig. 2. Ratio between inter-particle forces at suction s and at null suction due to water meniscus between two identical spheres (Fisher [65] curve scanned from Gallipoli et al. [15]).

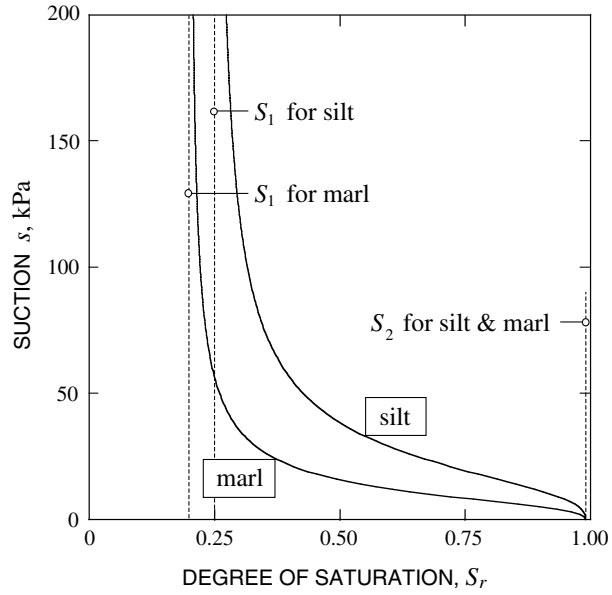

Fig. 3. Degree of saturation versus suction based on van Genuchten's [57] relation (parameters for silt and marl reported by Oettl et al. [3]).

In the fully saturated regime $c(\xi) = 1$, $a(\xi) = 0$, and $b(\xi) = 1$, and thus, $\overline{p}_c = p_c$. Thus, $p_c < 0$ is the *saturated* preconsolidation stress, the value which $\overline{p}_c$ tends to in the limit of full saturation. The word 'saturated' is used for p_c to suggest that it varies with the plastic deformation alone, and so it may be considered as the

plastic internal variable of the material model. The evolution of p_c may be obtained from the commonly used bilogarithmic compressibility law for a perfectly saturated soil,

$$v_{sat} = N - \tilde{\lambda} \ln p_c, \tag{4.15}$$

where N is the reference value of v_{sat} at unit saturated preconsolidation stress, and $\tilde{\lambda} > \tilde{\kappa}$ is the virgin compression index for the saturated soil. Solving for p_c and subtracting the elastic part gives the plastic hardening relation

$$\dot{p}_c = \frac{-p_c}{\tilde{\lambda} - \tilde{\kappa}} \operatorname{tr}(\dot{\boldsymbol{\epsilon}}^p). \tag{4.16}$$

Note that the sign of $\dot{p}_c$ follows the sign of $\operatorname{tr}(\dot{\boldsymbol{\epsilon}}^p)$: negative (hardening) under plastic compaction, i.e., the size of the yield surface is increasing, positive (softening) under plastic dilation, and perfect plasticity at the critical state.

A final component of the model is the flow rule defining the direction of the plastic strain rate. Alonso et al. [6] proposed a non-associative flow rule based on a plastic potential function G such that

$$\dot{\boldsymbol{\epsilon}}^p = \dot{\lambda} \frac{\partial G}{\partial \boldsymbol{\sigma}'} = \dot{\lambda} \left[\frac{1}{3}(2p' - p'_s - \overline{p}_c)\mathbf{1} + \frac{2q\beta}{M^2} \sqrt{\frac{3}{2}} \frac{\boldsymbol{s}}{\|\boldsymbol{s}\|} \right], \tag{4.17}$$

where β is a constant that can be derived by requiring that the direction of the plastic strain rate for zero lateral deformation agrees with the measured value of the coefficient of lateral stress K_0 at the one-dimensional constrained compression state (see Appendix 1 of [6]). If $\beta = 1$, then we have the case of associative plastic flow. The non-negative consistency parameter $\dot{\lambda}$ satisfies the standard Kuhn–Tucker loading–unloading conditions of plasticity theory.

4.2. Return mapping algorithm

From the standpoint of numerical integration at the local (Gauss point) level, the problem is to find the evolutions of $\boldsymbol{\sigma}'$ and p_c corresponding to prescribed incremental solid matrix strain tensor $\Delta\boldsymbol{\epsilon}$ and incremental matrix suction Δs, assuming their initial values are given at time t_n. For loading simulations characterized by a constant matrix suction s, the procedure is identical to the classical return mapping algorithm of computational plasticity. However, for a variable matrix suction the increment of s also must be prescribed in addition to the incremental strain tensor to drive the algorithm.

The steps necessary to carry out the return mapping algorithm for the constitutive model are summarized in Box 1. The box shows an operator split consisting of an elastic predictor followed by a plastic corrector, where the plastic corrector is triggered by the non-satisfaction of the yield criterion (Steps 1–3). If plastic yielding is detected in the elastic predictor phase, then the discrete plastic multiplier $\Delta\lambda$ is determined iteratively as elaborated in the following paragraphs. Note that $\boldsymbol{\epsilon}^{e\,tr}$, s, and ξ are all fixed during the local iteration phase (Step 4), although they themselves are iterated at the global (FE) level. Once $\Delta\lambda$ has been determined, the plastic corrector update can be performed (Step 5).

To accommodate stress-dependent elastic moduli in Step 4 of Box 1, it is convenient to perform the return mapping in the strain invariant space (see [34] for details). The idea is as follows. First, we pre-multiply (3.1) by the compliance tensor $(\boldsymbol{c}^e)^{-1}$ and integrate to obtain

$$\dot{\boldsymbol{\epsilon}}^e = \dot{\boldsymbol{\epsilon}} - \dot{\lambda} \frac{\partial G}{\partial \boldsymbol{\sigma}'} \Rightarrow \boldsymbol{\epsilon}^e = \boldsymbol{\epsilon}^{e\,tr} - \Delta\lambda \frac{\partial G}{\partial \boldsymbol{\sigma}'} \tag{4.18}$$

where $\boldsymbol{\epsilon}^{\mathrm{e}} = \boldsymbol{\epsilon}^{\mathrm{e}}_n + \Delta\boldsymbol{\epsilon}^{\mathrm{e}}$, $\boldsymbol{\epsilon}^{\mathrm{e\ tr}} = \boldsymbol{\epsilon}^{\mathrm{e}}_n + \Delta\boldsymbol{\epsilon}$, and $\Delta\lambda > 0$ is the discrete consistency parameter. The above equation can thus be viewed as a sequence of operations involving an elastic trial strain predictor followed by a plastic corrector. For two-invariant plasticity models we can reduce the above tensorial equation to a pair of scalar equations. Taking the volumetric and deviatoric parts gives

$$\epsilon^{\mathrm{e}}_{\mathrm{v}} = \epsilon^{\mathrm{e\ tr}}_{\mathrm{v}} - \Delta\lambda\frac{\partial G}{\partial p'}, \quad \boldsymbol{e}^{\mathrm{e}} = \boldsymbol{e}^{\mathrm{e\ tr}} - \Delta\lambda\frac{\partial G}{\partial \boldsymbol{s}}, \tag{4.19}$$

where $\partial G/\partial \boldsymbol{s} = (\partial G/\partial q)(3/2q)\boldsymbol{s}$. Now, since $\boldsymbol{e}^{\mathrm{e}}/\|\boldsymbol{e}^{\mathrm{e}}\| = \boldsymbol{s}/\|\boldsymbol{s}\|$ from the coaxiality of the elastic strain and effective constitutive stress tensors, the return mapping simplifies to a pair of scalar equations

$$\epsilon^{\mathrm{e}}_{\mathrm{v}} = \epsilon^{\mathrm{e\ tr}}_{\mathrm{v}} - \Delta\lambda\frac{\partial G}{\partial p'}, \quad \epsilon^{\mathrm{e}}_{\mathrm{s}} = \epsilon^{\mathrm{e\ tr}}_{\mathrm{s}} - \Delta\lambda\frac{\partial G}{\partial q}, \tag{4.20}$$

where $\epsilon^{\mathrm{e}}_{\mathrm{v}}$ and $\epsilon^{\mathrm{e}}_{\mathrm{s}}$ are defined in (4.5). Note that the normalized deviatoric tensor $\hat{\boldsymbol{n}} = \boldsymbol{e}^{\mathrm{e\ tr}}/\|\boldsymbol{e}^{\mathrm{e\ tr}}\| = \boldsymbol{e}^{\mathrm{e}}/\|\boldsymbol{e}^{\mathrm{e}}\|$ can be evaluated from the predictor values alone. From the flow rule (4.16), we easily get (see [34] for details)

$$\frac{\partial G}{\partial p'} = 2p' - p'_{\mathrm{s}} - \bar{p}_{\mathrm{c}}, \quad p' = p_0\exp\omega\left[1 + \frac{3\alpha}{2\tilde{\kappa}}(\epsilon^{\mathrm{e}}_{\mathrm{s}})^2\right], \tag{4.21a}$$

$$\frac{\partial G}{\partial q} = \frac{2\beta}{M^2}q, \quad q = 3(\mu_0 - \alpha p_0\exp\omega)\epsilon^{\mathrm{e}}_{\mathrm{s}}. \tag{4.21b}$$

Box 1. Return mapping algorithm for a hyperelastic–plastic constitutive model

Step 1. Compute $\boldsymbol{\epsilon}^{\mathrm{e\ tr}} = \boldsymbol{\epsilon}^{\mathrm{e}}_n + \Delta\boldsymbol{\epsilon}$; $\boldsymbol{e}^{\mathrm{e\ tr}} = \mathrm{dev}(\boldsymbol{\epsilon}^{\mathrm{e\ tr}})$; $\hat{\boldsymbol{n}} = \boldsymbol{e}^{\mathrm{e\ tr}}/\|\boldsymbol{e}^{\mathrm{e\ tr}}\|$; $s = s_n + \Delta s$; $S_r = S_r(s)$; $p'_{\mathrm{s}} = ks$; $\xi = f(s)(1 - S_r)$; calculate $c(\xi)$, $b(\xi)$, and $a(\xi)$.
Step 2. Elastic predictors: $\boldsymbol{\sigma}'^{\mathrm{tr}} = \partial\Psi^{\mathrm{e}}/\partial\boldsymbol{\epsilon}^{\mathrm{e\ tr}}$; $p^{\mathrm{tr}}_{\mathrm{c}} = p_{\mathrm{c},n}$; $\bar{p}^{\mathrm{tr}}_{\mathrm{c}} = -\exp[a(\xi)](-p^{\mathrm{tr}}_{\mathrm{c}})^{b(\xi)}$.
Step 3. Check if yielding: $F(\boldsymbol{\sigma}'^{\mathrm{tr}}, s, p^{\mathrm{tr}}_{\mathrm{c}}) > 0$?
No, set $\boldsymbol{\epsilon}^{\mathrm{e}} = \boldsymbol{\epsilon}^{\mathrm{e\ tr}}$; $p_{\mathrm{c}} = p^{\mathrm{tr}}_{\mathrm{c}}$ and exit.
Step 4. Yes, solve $F(\Delta\lambda) = 0$ for $\Delta\lambda$, see Box 2.
Step 5. Plastic correctors: $\boldsymbol{\epsilon}^{\mathrm{e}} = \epsilon^{\mathrm{e}}_{\mathrm{v}}\mathbf{1}/3 + \sqrt{3/2}\epsilon^{\mathrm{e}}_{\mathrm{s}}\hat{\boldsymbol{n}}$; $p_{\mathrm{c}} = p_{\mathrm{c},n}\exp[(\epsilon^{\mathrm{e}}_{\mathrm{v}} - \epsilon^{\mathrm{e\ tr}}_{\mathrm{v}})/(\tilde{\lambda} - \tilde{\kappa})]$ and exit.

So far the return mapping algorithm appears identical to the standard return maps for a Cam-Clay model. Below we show that the effect of partial saturation is to slightly alter the discrete consistency condition to include the presence of the matrix suction. First, we integrate (4.16) *exactly* to obtain the evolution of the saturated preconsolidation stress as

$$p_{\mathrm{c}} = p_{\mathrm{c},n}\exp\left(\frac{\epsilon^{\mathrm{e}}_{\mathrm{v}} - \epsilon^{\mathrm{e\ tr}}_{\mathrm{v}}}{\tilde{\lambda} - \tilde{\kappa}}\right), \tag{4.22}$$

where $p_{\mathrm{c},n}$ is the given value at the beginning of the load increment. Now, for a given matrix suction s we can calculate the corresponding bonding variable ξ and obtain the evolutions of p'_{s} and $\bar{p}_{\mathrm{c}}$, which we recall below as

$$p'_{\mathrm{s}} = ks, \quad \bar{p}_{\mathrm{c}} = -\exp[a(\xi)](-p_{\mathrm{c}})^{b(\xi)}. \tag{4.23}$$

Imposing the discrete consistency condition then gives

$$F = \frac{q^2}{M^2} + (p' - p'_{\mathrm{s}})(p' - \bar{p}_{\mathrm{c}}) = 0, \tag{4.24}$$

where p' and q are defined in terms of the volumetric and deviatoric elastic strain invariants alone, according to (4.21), but are otherwise unaffected by the matrix suction s. Thus, s affects the return mapping algorithm only through the variables p'_s and $\overline{p}_c$ of the discrete consistency condition.

To solve for $\Delta\lambda$ in Step 4 of Box 1, we construct a residual vector $\boldsymbol{r}$ and a vector of unknowns $\boldsymbol{x}$, with elements

$$\boldsymbol{r} = \begin{Bmatrix} \epsilon_v^e - \epsilon_v^{e\,tr} + \Delta\lambda\, \partial_{p'} G \\ \epsilon_s^e - \epsilon_s^{e\,tr} + \Delta\lambda\, \partial_q G \\ F \end{Bmatrix}, \quad \boldsymbol{x} = \begin{Bmatrix} \epsilon_v^e \\ \epsilon_s^e \\ \Delta\lambda \end{Bmatrix}. \tag{4.25}$$

The driving forces in this problem are the fixed trial elastic strains $\epsilon_v^{e\,tr}$ and $\epsilon_s^{e\,tr}$, and the matrix suction s. Note that even in the absence of imposed incremental strains a residual component could result from prescribing an incremental matrix suction s, thus violating the discrete consistency condition and driving the iterative algorithm. This would be the case, for example, when the matrix suction is reduced resulting in a 'wetting collapse' phenomenon as elaborated in [6].

To dissipate the residual vector we need a tangent operator for local Newton iteration. In the following we shall adopt the procedure in [34] and construct such a consistent tangent operator, highlighting precisely where the matrix suction enters into the algorithm. First, we recall the elastic tangential relation

$$\begin{Bmatrix} \delta p' \\ \delta q \end{Bmatrix} = \boldsymbol{D}^e \begin{Bmatrix} \delta\epsilon_v^e \\ \delta\epsilon_s^e \end{Bmatrix}, \tag{4.26}$$

where $\boldsymbol{D}^e$ is a 2×2 Hessian matrix of Ψ^e of the form

$$\boldsymbol{D}^e = \begin{bmatrix} D_{11}^e & D_{12}^e \\ D_{21}^e & D_{22}^e \end{bmatrix} = \begin{bmatrix} \partial^2_{\epsilon_v^e \epsilon_v^e} & \partial^2_{\epsilon_v^e \epsilon_s^e} \\ \partial^2_{\epsilon_s^e \epsilon_v^e} & \partial^2_{\epsilon_s^e \epsilon_s^e} \end{bmatrix} \Psi^e = \begin{bmatrix} -p'/\tilde{\kappa} & (3p_0\alpha\epsilon_s^e/\tilde{\kappa})\exp\omega \\ (3p_0\alpha\epsilon_s^e/\tilde{\kappa})\exp\omega & 3\mu^e \end{bmatrix}. \tag{4.27}$$

Next, we define a 2×2 Hessian matrix of the plastic potential function G of the form

$$\boldsymbol{H} = \begin{bmatrix} H_{11}^e & H_{12}^e \\ H_{21}^e & H_{22}^e \end{bmatrix} = \begin{bmatrix} \partial^2_{p'p'} & \partial^2_{p'q} \\ \partial^2_{qp'} & \partial^2_{qq} \end{bmatrix} G = \begin{bmatrix} 2 & 0 \\ 0 & 2\beta/M^2 \end{bmatrix}, \tag{4.28}$$

from which we construct

$$\boldsymbol{K} = \begin{bmatrix} K_{11} & K_{12} \\ K_{21} & K_{22} \end{bmatrix} := \boldsymbol{H}\boldsymbol{D}^e. \tag{4.29}$$

The consistent tangent operator then takes the form

$$\boldsymbol{r}'(\boldsymbol{x}) = \begin{bmatrix} 1 + \Delta\lambda(K_{11} + K_p \partial^2_{p'\overline{p}_c} G) & \Delta\lambda K_{12} & \partial_{p'} G \\ \Delta\lambda(K_{21} + K_p \partial^2_{q\overline{p}_c} G) & 1 + \Delta\lambda K_{22} & \partial_q G \\ D_{11}^e \partial_{p'} F + D_{21}^e \partial_q F + K_p \partial_{\overline{p}_c} F & D_{12}^e \partial_{p'} F + D_{22}^e \partial_q F & 0 \end{bmatrix}, \tag{4.30}$$

where $\partial_{p'} F = \partial_{p'} G = 2p' - p'_s - \overline{p}_c$; $\partial_q F = 2q/M^2$; $\partial_q G = 2\beta q/M^2$; $\partial_{\overline{p}_c} F = -(p' - p'_s)$; $\partial^2_{p'\overline{p}_c} G = -1$; $\partial^2_{q\overline{p}_c} G = 0$; and $K_p = \partial\overline{p}_c/\partial\epsilon_v^e = b(\xi)\overline{p}_c/(\tilde{\lambda} - \tilde{\kappa})$. The form for $\boldsymbol{r}'(\boldsymbol{x})$ is clearly similar to that employed in [34] for the standard Cam-Clay return mapping, the only major difference being that the effective preconsolidation stress $\overline{p}_c$ is now used for the partially saturated formulation. This suggests that from the implementational standpoint the present (local) stress-point integration algorithm is practically the same as that used for the perfectly saturated Cam-Clay model. However, some additional coding effort may be required at the global level to consistently linearize the suction term, in addition to the elastic trial strains, which were both held fixed at the local iteration level.

The local Newton iteration algorithm is summarized in Box 2. Once the converged value of $\boldsymbol{x}$, denoted as $\boldsymbol{x}^*$ in Box 2, has been determined, the elastic strain tensor for the solid matrix can be calculated as

$$\boldsymbol{\epsilon}^{\mathrm{e}} = \frac{1}{3}\epsilon_{\mathrm{v}}^{\mathrm{e}}\mathbf{1} + \sqrt{\frac{3}{2}}\epsilon_{\mathrm{s}}^{\mathrm{e}}\hat{\boldsymbol{n}}, \tag{4.31}$$

from which the effective constitutive Cauchy stress tensor is obtained as

$$\boldsymbol{\sigma}' = p'\mathbf{1} + \sqrt{\frac{2}{3}}q\hat{\boldsymbol{n}}, \tag{4.32}$$

where $\hat{\boldsymbol{n}} = \boldsymbol{e}^{\mathrm{e\,tr}}/\|\boldsymbol{e}^{\mathrm{e\,tr}}\|$.

Box 2. Structure of local Newton iteration algorithm. Typical value of etol $<10^{-10}$

Step 1. Initialize $k = 0$; $\Delta\lambda^k = 0$; $\epsilon_{\mathrm{v}}^{\mathrm{e},k} = \epsilon_{\mathrm{v}}^{\mathrm{e\,tr}}$; $\epsilon_{\mathrm{s}}^{\mathrm{e},k} = \epsilon_{\mathrm{s}}^{\mathrm{e\,tr}}$.
Step 2. Assemble $\boldsymbol{r}(\boldsymbol{x}^k)$.
Step 3. Check convergence: $\|\boldsymbol{r}(\boldsymbol{x}^k)\| \leqslant \mathrm{etol}\|\boldsymbol{r}(\boldsymbol{x}^0)\|$?
Yes, set $\boldsymbol{x}^* = \boldsymbol{x}^k$ and exit.
Step 4. No, construct $\boldsymbol{a} = \boldsymbol{r}'(\boldsymbol{x}^k)$.
Step 5. Set $\boldsymbol{x}^{k+1} = \boldsymbol{x}^k - \boldsymbol{a}^{-1}\cdot\boldsymbol{r}(\boldsymbol{x}^k)$; $k = k + 1$; and go to Step 2.

4.3. Constitutive tangent operators

In this section we develop expressions for the drained and undrained constitutive tangent operators useful for the construction of the corresponding elastoplastic acoustic tensors.

We also describe how the matrix suction impacts the condition for the onset of a deformation band. First, we recall from (3.16) the following expression for the drained elastoplastic constitutive operator $\boldsymbol{c}^{\mathrm{ep}}$ relating the effective constitutive Cauchy stress rate $\dot{\boldsymbol{\sigma}}'$ to the solid matrix strain rate $\dot{\boldsymbol{\epsilon}}$,

$$\boldsymbol{c}^{\mathrm{ep}} = \boldsymbol{c}^{\mathrm{e}} - \frac{1}{\chi}\boldsymbol{c}^{\mathrm{e}} : \boldsymbol{g}\otimes\boldsymbol{f} : \boldsymbol{c}^{\mathrm{e}}, \quad \chi = \boldsymbol{f} : \boldsymbol{c}^{\mathrm{e}} : \boldsymbol{g} + H. \tag{4.33}$$

The tangential elasticity tensor $\boldsymbol{c}^{\mathrm{e}}$ has the explicit form [34]

$$\boldsymbol{c}^{\mathrm{e}} = K^{\mathrm{e}}\mathbf{1}\otimes\mathbf{1} + 2\mu^{\mathrm{e}}\left(\boldsymbol{I} - \frac{1}{3}\mathbf{1}\otimes\mathbf{1}\right) + \sqrt{\frac{2}{3}}d^{\mathrm{e}}(\mathbf{1}\otimes\hat{\boldsymbol{n}} + \hat{\boldsymbol{n}}\otimes\mathbf{1}), \tag{4.34}$$

where $K^{\mathrm{e}} = -p'/\tilde{\kappa} > 0$ is the tangential elastic bulk modulus, $\mu^{\mathrm{e}} = \mu_0 - \alpha p_0\exp\omega > 0$ is the tangential elastic shear modulus, $d^{\mathrm{e}} = (3p_0\alpha\epsilon_{\mathrm{s}}^{\mathrm{e}}/\tilde{\kappa})\exp\omega < 0$ is a tangential coupling modulus, $\boldsymbol{I}$ is the rank-four identity tensor, and $\hat{\boldsymbol{n}} = \boldsymbol{e}^{\mathrm{e}}/\|\boldsymbol{e}^{\mathrm{e}}\|$. Note that if $d^{\mathrm{e}} \neq 0$ an elastic coupling between the volumetric and deviatoric responses is generated due to enforcing a linear dependence of K^{e} and μ^{e} on the mean normal stress p'; otherwise, if $d^{\mathrm{e}} = 0$ no such coupling exists, which would be the case if $\mu^{\mathrm{e}} = \mu_0 = \text{constant}$. Since the elastic response is assumed independent of the suction, $\boldsymbol{c}^{\mathrm{e}}$ is the same for partially and fully saturated cases.

The chain rule on the yield function gives

$$\boldsymbol{f} = \frac{\partial F}{\partial\boldsymbol{\sigma}'} = \frac{1}{3}\left(\frac{\partial F}{\partial p'}\right)\mathbf{1} + \sqrt{\frac{3}{2}}\left(\frac{\partial F}{\partial q}\right)\hat{\boldsymbol{n}}, \tag{4.35}$$

where

$$\frac{\partial F}{\partial p'} = 2p' - p_{\mathrm{s}}' - \bar{p}_{\mathrm{c}}, \quad \frac{\partial F}{\partial q} = \frac{2q}{M^2}. \tag{4.36}$$

The plastic flow direction takes a similar form,

$$\boldsymbol{g} = \frac{\partial G}{\partial \boldsymbol{\sigma}'} = \frac{1}{3}\left(\frac{\partial F}{\partial p'}\right)\mathbf{1} + \sqrt{\frac{3}{2}}\left(\beta\frac{\partial F}{\partial q}\right)\hat{\boldsymbol{n}}, \tag{4.37}$$

where β is the non-associativity parameter. In both $\boldsymbol{f}$ and $\boldsymbol{g}$ the matrix suction enters only through the variables p'_{s} and $\overline{p}_{\mathrm{c}}$.

Completing the formulation, the scalar product in the expression for χ simplifies to

$$\boldsymbol{f} : \boldsymbol{c}^{\mathrm{e}} : \boldsymbol{g} = K^{\mathrm{e}}\left(\frac{\partial F}{\partial p'}\right)^2 + d^{\mathrm{e}}(1+\beta)\left(\frac{\partial F}{\partial p'}\frac{\partial F}{\partial q}\right) + 3\beta\mu^{\mathrm{e}}\left(\frac{\partial F}{\partial q}\right)^2 > 0. \tag{4.38}$$

For this product to be strictly positive β must not be too different from unity, thus imposing a limit on the severity of the non-associative plastic flow. Finally, the plastic modulus H for the constitutive model simplifies to

$$H = \frac{\partial F}{\partial \overline{p}_{\mathrm{c}}}\frac{\partial F}{\partial p'}\frac{b(\xi)}{\tilde{\lambda}-\tilde{\kappa}}\overline{p}_{\mathrm{c}}, \quad \frac{\partial F}{\partial \overline{p}_{\mathrm{c}}} = -(p' - p'_{\mathrm{s}}) > 0. \tag{4.39}$$

In the limit of full saturation $\overline{p}_{\mathrm{c}} = p_{\mathrm{c}}$, $p'_{\mathrm{s}} = 0$, and $b(\xi) = 1$. Since $|\overline{p}_{\mathrm{c}}| > |p_{\mathrm{c}}|$, the effect of partial saturation is to increase the absolute value of the plastic modulus relative to its value in the fully saturated case. In other words, the suction amplifies the hardening response on the compactive side of the yield surface, as well as amplifies the softening response on the dilatant side. These features in turn influence the deformation and strain localization behavior of the material, as demonstrated in the next section.

For the locally undrained condition we recall from (4.19)–(4.21) the undrained elastoplastic constitutive operator $\tilde{\boldsymbol{c}}^{\mathrm{ep}}$ for the total mixture,

$$\tilde{\boldsymbol{c}}^{\mathrm{ep}} = \boldsymbol{c}^{\mathrm{ep}} + \frac{\varphi}{\chi}(\bar{\lambda}^{\mathrm{a}} - \bar{\lambda}^{\mathrm{w}})\boldsymbol{c}^{\mathrm{e}} : \boldsymbol{g}\otimes\mathbf{1} + \bar{\lambda}^{\mathrm{v}}\mathbf{1}\otimes\mathbf{1}, \tag{4.40}$$

where $\boldsymbol{c}^{\mathrm{ep}}$ is the elastoplastic constitutive operator for the underlying drained solid and $\bar{\lambda}^{\mathrm{v}}$ is a Lamé-like parameter representing the weighted bulk response of the water and air phases in the void. We note that the second term on the right-hand side arises from the suction-dependence of the constitutive model for the drained solid, which destroys the symmetry of the constitutive operator for the entire mixture. The third term arises from an additive decomposition of the total stress into a constitutive effective stress and linear fractions of the pore air and pore water pressures. Below we outline the relevant derivatives necessary to evaluate the operator $\tilde{\boldsymbol{c}}^{\mathrm{ep}}$.

By definition,

$$\varphi = \frac{\partial F}{\partial s} = -(p' - \overline{p}_{\mathrm{c}})\frac{\partial p'_{\mathrm{s}}}{\partial s} - (p' - p'_{\mathrm{s}})\frac{\partial \overline{p}_{\mathrm{c}}}{\partial s}, \tag{4.41}$$

where

$$\frac{\partial p'_{\mathrm{s}}}{\partial s} = k, \quad \frac{\partial \overline{p}_{\mathrm{c}}}{\partial s} = \frac{\partial \overline{p}_{\mathrm{c}}}{\partial \xi}\xi'(s). \tag{4.42}$$

We recall that $\overline{p}_{\mathrm{c}} = \overline{p}_{\mathrm{c}}(p_{\mathrm{c}}, \xi(s))$, and p_{c} is the preconsolidation stress at full saturation and so is not a function of s, which explains the second part of (4.42). Differentiating $\overline{p}_{\mathrm{c}}$ with respect to the bonding variable ξ gives

$$\frac{\partial \overline{p}_{\mathrm{c}}}{\partial \xi} = \overline{p}_{\mathrm{c}}[a'(\xi) + b'(\xi)\ln(-p_{\mathrm{c}})], \tag{4.43}$$

where

$$a'(\xi) = \frac{Nb(\xi)}{\tilde{\lambda}c(\xi) - \tilde{\kappa}}c'(\xi), \quad b'(\xi) = \frac{-\tilde{\lambda}b(\xi)}{\tilde{\lambda}c(\xi) - \tilde{\kappa}}c'(\xi), \quad c'(\xi) = c_1c_2\exp(c_2\xi). \tag{4.44}$$

Finally, we obtain from (4.11) the derivative of the bonding variable ξ with respect to s as

$$\xi'(s) = (1 - S_r)f'(s) - f(s)S_r'(s), \tag{4.45}$$

where

$$f'(s) = \frac{10.7/p_{\text{atm}}}{[10.7 + 2.4(s/p_{\text{atm}})]^2} \tag{4.46}$$

and

$$S_r'(s) = -(S_2 - S_1)\left(\frac{mn}{s_{\text{a}}}\right)\left(\frac{s}{s_{\text{a}}}\right)^{n-1}\left[1 + \left(\frac{s}{s_{\text{a}}}\right)^n\right]^{-(m+1)}. \tag{4.47}$$

The above tangential relationship for $S_r'(s)$ is also necessary for evaluating the coefficients $\bar{\lambda}^{\text{a}}$ and $\bar{\lambda}^{\text{w}}$.

4.4. Some remarks on non-convexity of the yield function

Recently, some authors [53,54] have noted an important implication of the failure of many plasticity models for partially saturated soils to satisfy the criteria for maximum plastic dissipation, that of non-convexity of the resulting yield function. This feature manifests itself on a so-called loading collapse (LC) yield curve representing the plot of the yield function on the p'–s plane, as depicted in Fig. 4. The lack of convexity occurs along the suction axis near the transition zone from a perfectly saturated state to a partially saturated state ($s \approx 0$). Wheeler et al. [53] noted (p. 1569) that there is no conclusive experimental evidence to show whether non-convex sections of LC yield curve do occur in practice, but this feature is likely to cause practical problems in numerical analysis employing a stress return mapping algorithm. *This is not so*.

From a numerical standpoint, the lack of convexity of a yield function could result in two types of problems: (a) with a large load increment the elastic stress predictor could overshoot the plastic region on the non-convex side resulting in an underestimation of the cumulative plastic strain (Fig. 4); and (b) the algorithm could result in a non-unique plastic return map due to the existence of more than one normal plastic direction to the yield surface on the non-convex side. The first problem can, of course, be circumvented trivially by reducing the load increment. The second problem is more serious for a general non-convex yield surface. However, the non-convexity pointed out in [53,54] occurs only on the suction axis, and since the suction stress s is held fixed during the plastic corrector phase (see Box 1), the return direction is unique (provided of course that the yield function $F(\boldsymbol{\sigma}', s, p_{\text{c}}) = 0$ is convex for a fixed s). We recall that $s = p_{\text{a}} - p_{\text{w}}$, and s can only be determined on the global level by applying field equations to determine p_{a} and p_{w}. In other words, on the local level there is no return map on the suction axis that causes the numerical problem pointed out in [53,54].

5. Simulations

In this section we illustrate the features of the constitutive model at the local level, including its strain localization properties. Following the simulation procedure presented in [62], we prescribe different strain and matrix suction histories and demonstrate the model response along with the performance of the return mapping algorithm. We emphasize that a complete analysis of the boundary-value problem has the deformation and matrix suction (through the pore air and pore water pressures) as the unknowns, but the performance of the global algorithm relies heavily on what happens at the local level, which is why we have chosen a deformation/suction-driven format for the present simulations.

The assumed hyperelastic model parameters are: $\tilde{\kappa} = 0.03$, $\epsilon_{\text{v0}}^{\text{e}} = 0$, $\alpha = 103$, and $\mu_0 = 0$. The elastic volumetric and deviatoric responses are thus coupled, with a coupling parameter α taking on a value similar

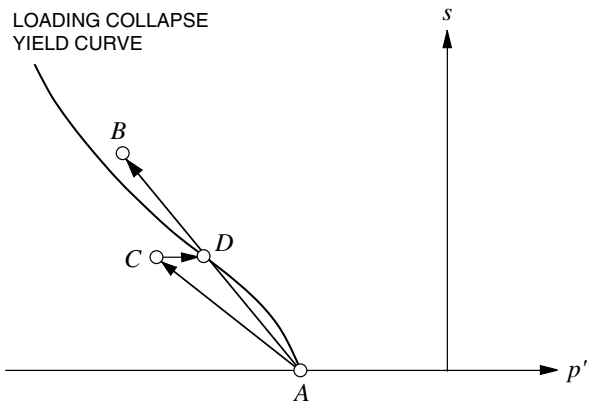

Fig. 4. Non-convexity of loading collapse yield curve: elastic predictor AB overshoots the plastic region on the non-convex side; elastic predictor AC detects yielding on the non-convex side and returns to a unique map CD at constant suction s.

to that determined for Vallericca clay [35]. The assumed plasticity model parameters are $M = 1.0$, $\tilde{\lambda} = 0.11$, $N = 2.76$, $k = 0.6$, and $\beta = 1.0$. These values are approximately the same as those quoted in [6,15] from model calibration utilizing laboratory test data (the assumed value of β results in associative plasticity, so we shall study the influence of non-associativity by varying this parameter). The assumed van Genuchten function parameters are: $S_1 = 0.25$, $S_2 = 1.00$, $s_a = 20$ kPa, $n = 2.5$, and $m = 0.6$. These values are the same as those used in [2,3] for silt, with the exception that they assumed $S_2 = 0.99$ (the assumed value of $S_2 = 1.00$ allows the preconsolidation stress $\overline{p}_c$ to reach a value exactly equal to p_c at zero suction). The fitting parameter values in the Gallipolli et al. [15] curve are $c_1 = 0.185$ and $c_2 = 1.42$.

5.1. Isotropic stress relaxation due to loss of suction

We assume initial elastic strain $\boldsymbol{\epsilon}^e = \mathbf{0}$, initial suction $s = 20$ kPa, initial preconsolidation pressure $p_c = -10$ kPa, and $p_0 = -20$ kPa. This leads to initial isotropic stresses $\sigma'_{11} = \sigma'_{22} = \sigma'_{33} = -20$ kPa, initial bonding variable $\xi = 0.250$, and initial effective preconsolidation $\overline{p}_c = -92.7$ kPa; hence the stress point is initially well inside the elastic region. We then decrease the suction in increments of 0.5 kPa while keeping the total strains fixed. Fig. 5 shows the movement of $\overline{p}_c$ as the suction is decreased from its initial value at point a until it meets the stress point at b. During this time the zero-suction zone remains stationary, represented by the dark shaded semi-ellipse on the p'–q plane passing through point d. As the suction is reduced further beyond point b, where $\xi = 0.078$, the stress point 'relaxes' to c, where $\xi = 0$, while the zero-suction zone concurrently expands to the light shaded semi-ellipse passing through point c due to compative plastic strain induced by the loss of suction. This phenomenon is called 'wetting-collapse mechanism' (see e.g., [6]). If the material had not yielded, the movement of $\overline{p}_c$ beyond point b would have been denoted by the dashed curve b–d on the v–p' plane as shown in Fig. 5.

5.2. Deviatoric stress relaxation due to loss of suction

We assume initial elastic strains $\epsilon^e_{11} = -\epsilon^e_{22} = 0.00351$, initial suction $s = 20$ kPa, and initial preconsolidation pressure $p_c = -100$ kPa, and $p_0 = -100$ kPa. This leads to initial $p' = -108.6$ kPa, $q = 126.1$ kPa, $\xi = 0.250$, and $\overline{p}_c = -740.4$ kPa. We then decrease the suction in increments of 0.5 kPa while keeping

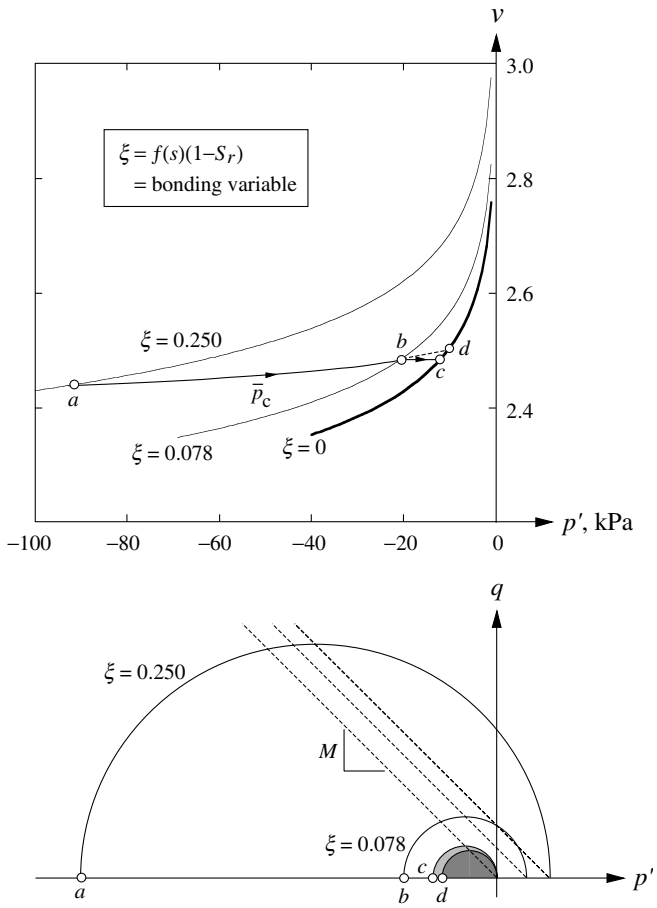

Fig. 5. Simulation of isotropic stress relaxation induced by loss of suction.

the total strains fixed. Fig. 6 shows the stress point relaxing from b to c as ξ decreases from 0.113 to zero (point b remains stationary while ξ decreases from 0.250 to 0.113). Concurrently, the zero-suction zone denoted by the dark shaded semi-ellipse on the p'–q plane slightly increases in size as the stress point relaxes to a fully saturated state at point c. The stress path b–c is nearly vertical on the p'–q plane signifying a nearly deviatoric stress relaxation. Consequently, b, c and d cluster together at the same point on the v–p' plane. This example demonstrates that the stress point can relax from a nearly critical state (point b) to a nearly isotropic state (point c) simply by varying the matrix suction.

The convergence profiles of the iterative algorithm for Examples 5.1 and 5.2 are shown in Fig. 7. Asymptotic quadratic rate of convergence is achieved in all the time steps requiring an iterative solution (i.e., when the material undergoes plasticity).

5.3. Constrained compression combined with loss of suction

In this example we assume the same material parameters and initial conditions as in Example 5.2. However, at each time step we now impose an incremental strain $\Delta\epsilon_{22} = -0.001$ holding all the other strain

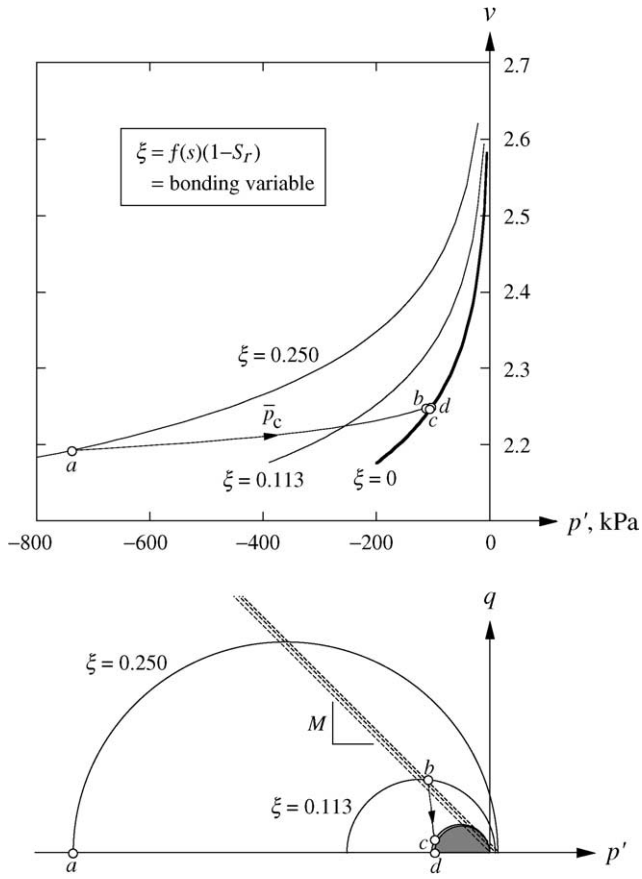

Fig. 6. Simulation of nearly deviatoric stress relaxation induced by loss of suction.

components fixed (constrained compression on the 2-axis), and concurrently apply an incremental suction $\Delta s = -0.5$ kPa. Fig. 8 shows the results of the simulations. Starting from the initial point a, the material loads elastically to point b while the bonding variable decreases from an initial value $\xi = 0.250$ to an intermediate value $\xi = 0.211$. Thereafter, elastoplastic deformation takes place due to simultaneous loading and loss of suction, represented by the curve b–c. Note an apparent softening along this path showing the dominant effect of loss of suction, even when the stress point already lies on the compactive side of the yield surface causing the zero-suction zone to expand from the dark shaded semi-ellipse to a light shaded one on the p'–q plane. At point c full saturation is achieved and the suction can no longer decrease. Path c–d then shows plastic loading by constrained compression at full saturation, which is accompanied by expansion of the fully saturated zone denoted by the lighter shaded semi-ellipse on the p'–q plane. Note in this case that in the fully saturated regime the zero-suction zone and the elastic region are the same (since $S_2 = 1.0$ and thus, $\bar{p}_c = p_c$ at full saturation). The convergence profiles of the local Newton iterations for this particular example are shown in Fig. 9.

5.4. Accuracy analysis: 3D loading with increasing suction

Here, we assume the same material parameters and initial conditions as in Example 5.2 except that the initial suction is now zero. We then impose total additional strains $\epsilon_{22} = -0.10$ and $\gamma_{12} = 2\epsilon_{12} = 0.08$ (all the

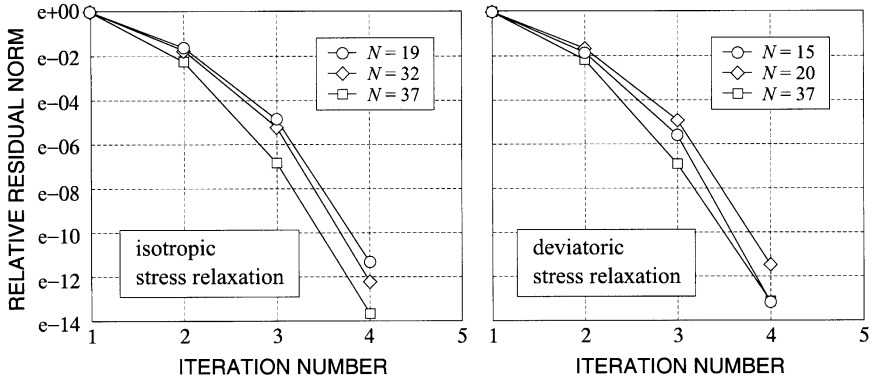

Fig. 7. Convergence profile of local Newton iterations for stress relaxation simulations induced by loss of suction.

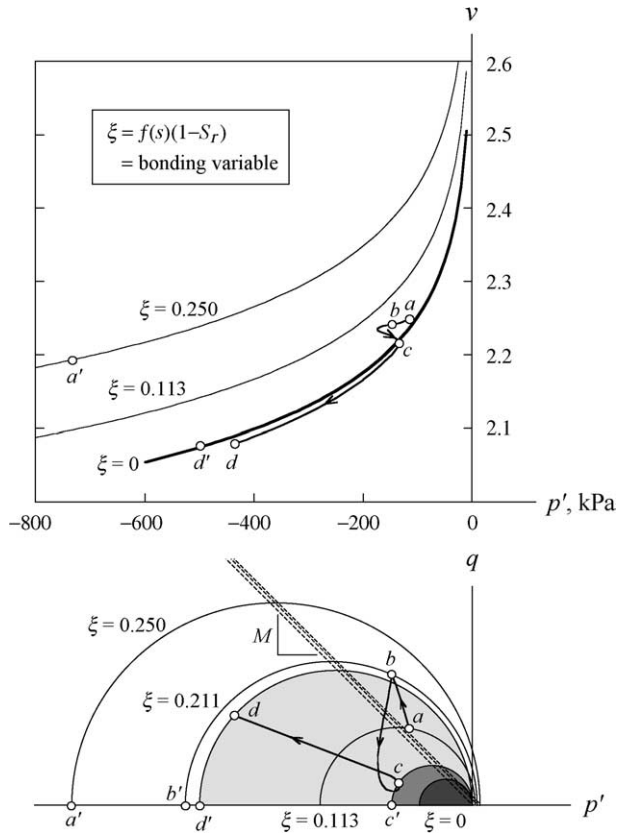

Fig. 8. Simulation of constrained compression loading combined with loss of suction. Stress path denoted by *a–b–c–d*.

other strain components are fixed), and total suction of $s = 20$ kPa in four, 40 and 400 equal increments. The objective of this study is to investigate the accuracy of the integration algorithm by varying the step size. Fig. 10 shows a comparison of the predicted stress paths on the p'–q plane. The 40-step and 400-step

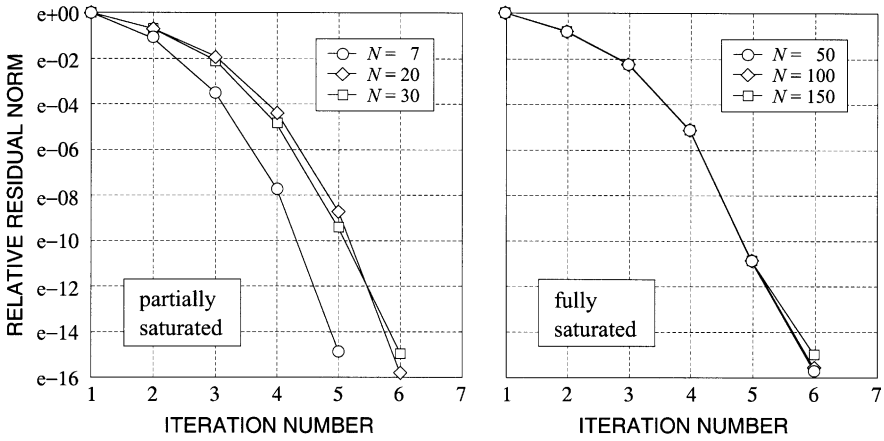

Fig. 9. Convergence profile of local Newton iterations for combined constrained compression loading-loss of suction simulation.

solutions are nearly the same; in fact, even the excessively coarse discretization consisting of only four increments resulted in a stress path that is quite close to the 'exact' solution and well demonstrates the accuracy of the integration algorithm. Note the pronounced effect of suction on the size of the yield surface as the size of the zero-suction zone, p_c, easily lags the size of the yield surface, $\overline{p}_c$, even for this modest increase of the matrix suction ($\overline{p}_c = p_c$ initially, representing the size of the dark shaded semi-ellipse). Also worthy of note is the stiffer response at higher values of suction exhibited by the model, which is very much evident from the four-step solution where despite the fact that the strains and suction were applied in equal increments the resulting stress increments increased with increasing suction.

# steps	p_c	$\overline{p}_c$
400	−170.587	−1299.162
40	−170.311	−1297.273
4	−167.579	−1278.565

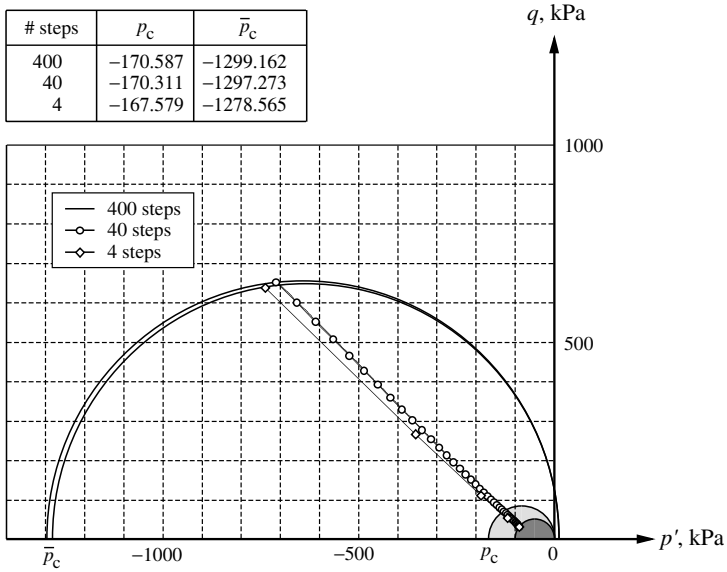

Fig. 10. Accuracy analysis for combined 3D loading-increase in suction simulation: shaded semi-ellipses denote yield surfaces at full saturation.

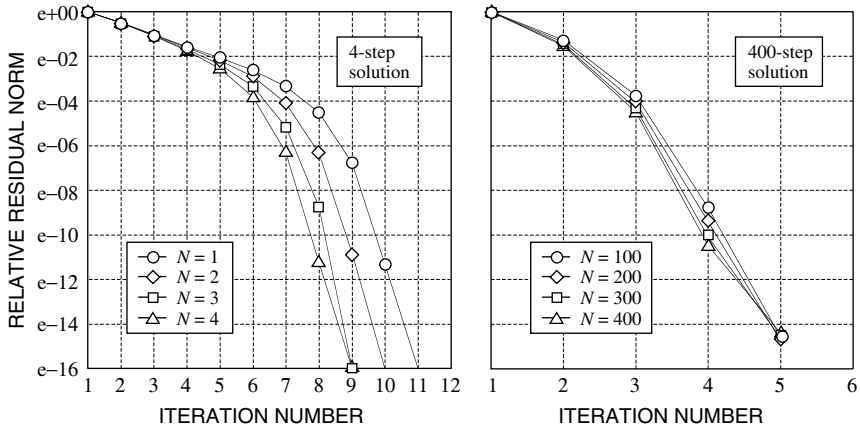

Fig. 11. Convergence profile of local Newton iterations for 4-step and 400-step solutions: combined 3D loading-increase in suction simulation.

The convergence profiles of the local Newton iterations are compared in Fig. 11 for the 4-step and 400-step solutions. The figure shows an increase in the number of iterations per increment as the increment size increases, which is to be expected in a non-linear analysis of this nature. Otherwise, the iterations demonstrate the expected asymptotic rate of quadratic convergence irrespective of the size of the load increment.

5.5. Shear band analysis: drained case

For this example we assume the same material parameters and initial conditions as in Example 5.2, and impose incremental strains $\Delta\epsilon_{11} = 0.0005$, $\Delta\epsilon_{22} = -0.001$, all other $\Delta\epsilon_{ij}$'s = 0 (plane strain on the 12-plane). In the first simulation we assume a constant suction, while in the second simulation we assume $\Delta s = -0.5$ kPa. As shown in Fig. 6 the initial stress point lies slightly on the dilatant side of the critical state, and remains on that side until the moment of initial yielding. As the yield surface shrinks due to softening induced by plastic dilatancy for the constant suction simulation, combined with the loss of suction for the decreasing suction simulation, the stress point moves toward the compactive side of the yield surface. Fig. 12(a) shows that at the moment of initial yielding (step number $N = 7$) negative determinants of the drained elastoplastic acoustic tensor are detected immediately over a relatively wide range of band orientations, but as the stress point moves toward the compactive side the determinants become all positive as the plastic modulus switches in sign from negative to positive. For the case of decreasing suction initial yielding occurs at an earlier stage ($N = 5$), as shown in Fig. 12(b), at which instant nearly zero determinants of the drained elastoplastic acoustic tensor are detected at band orientations approximately 44° and 136° on the plane of the problem (orientations of band normal vector $\boldsymbol{n}$ relative to the x_1-plane). At these band normals, the orientation of the instantaneous velocity jump vector $\boldsymbol{m}$ are −44° and 44°, respectively, suggesting a nearly isochoric shear band since $\boldsymbol{n} \cdot \boldsymbol{m} \approx 0$ (see [22,23] for a discussion of various types of deformation bands). This is consistent with the fact that bifurcation occurs near the critical state. However, the determinants immediately become all positive as the stress point moves toward the compactive side of the yield surface.

To demonstrate the effect of non-associativity, we assume a non-associativity parameter $\beta = 0.5$. This value was calculated using Eq. (42) of Alonso et al. [6], where β was expressed in terms of the parameters M, $\tilde{\lambda}$ and $\tilde{\kappa}$ satisfying a certain relationship for zero lateral deformation. The effect of having β less than

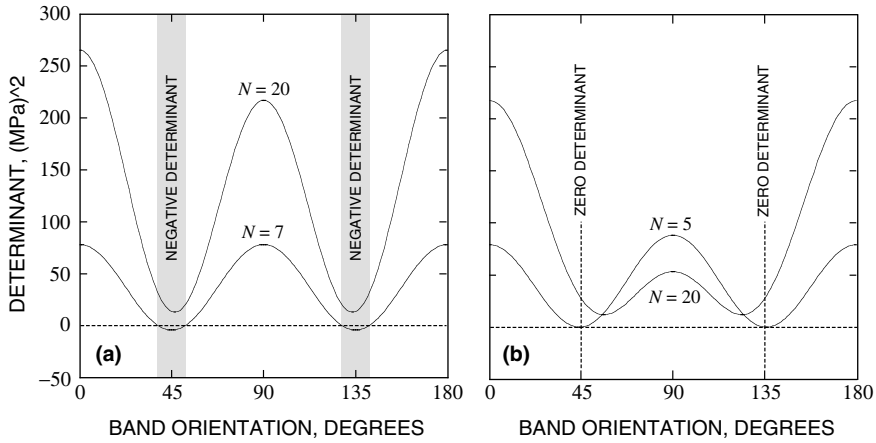

Fig. 12. Variation of determinant function with band orientation $\beta = 1.0$: (a) drained bifurcation near the critical state at constant suction; (b) drained bifurcation near the critical state at decreasing suction.

unity is to reduce the magnitude of the incremental deviatoric plastic strain relative to the incremental volumetric plastic strain. Fig. 13 shows the variations of the determinant function demonstrating a wider range of band orientations with negative determinants compared to the associative plasticity case (cf. Fig. 12). This is consistent with the well known result that for a shear band mode non-associative plasticity enhances the loss of strong ellipticity of the acoustic tensor.

5.6. Shear band analysis: undrained case

In this example we illustrate the competing effects on the localization properties of the following additional terms comprising the undrained elastoplastic constitutive operator $\tilde{\boldsymbol{c}}^{\mathrm{ep}}$ of a three-phase medium (cf.

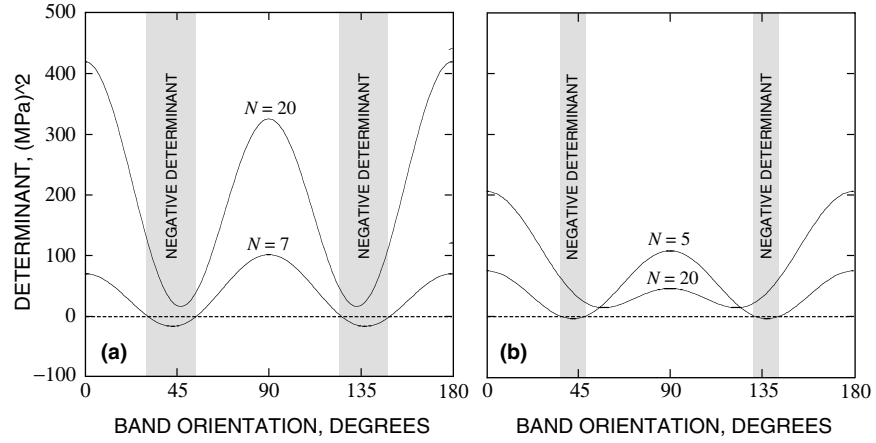

Fig. 13. Variation of determinant function with band orientation, $\beta = 0.50$: (a) drained bifurcation near the critical state at constant suction; (b) drained bifurcation near the critical state at decreasing suction.

(4.40)): (a) the unsymmetric term $\varphi(\bar{\lambda}^{a} - \bar{\lambda}^{w})\boldsymbol{c}^{e} : \boldsymbol{g} \otimes \mathbf{1}/\chi$ which enhances the formation of a shear band relative to the drained case; and (b) the weighted bulk modulus term $\bar{\lambda}^{v}\mathbf{1} \otimes \mathbf{1}$ of the void which delays the onset of a shear band when yielding on the dilatant side of the yield surface. It is well known that a non-associative flow rule favors the development of a shear band because it destroys the symmetry of the constitutive tangent operator [21]; thus, the presence of the unsymmetric term (a) is expected to have the same effect of enhancing the onset of a shear band. On the other hand, it is also well known that for dilatant frictional materials drained localization precedes undrained localization since the presence of fluids in the voids introduces a volume constraint that enables a frictional material to gain strength [24]; hence, on the dilatant side of the yield surface the symmetric bulk term (b) generates the same volume constraint that delays the onset of a shear band.

To illustrate the effect of the volume constraint on the onset of a shear band we repeat the analyses of Example 5.5 and investigate the loss of strong ellipticity of the acoustic tensor at the end of each time step utilizing the undrained constitutive operator $\tilde{\boldsymbol{c}}^{ep}$ for the total mixture. Care must be exercised when intepreting the results of these analyses since, strictly speaking, we are not simulating an undrained deformation response but are simply comparing the localization properties of the drained and undrained constitutive operators at the same effective stress point. From a physical standpoint the simulation is equivalent to applying a load increment instantaneously at the beginning of each time step and allowing the material to drain (or 'consolidate') before applying the next instantaneous load increment, i.e., the load-time history is a step function. Fig. 14 shows the resulting determinant functions at different band orientations. Compared with Fig. 13 we observe narrower ranges of band orientation at which the determinant function is negative at initial yield. This suggests that the effect of the symmetric bulk term (b) is more dominant than the effect of the unsymmetric term (a) for this particular example.

Finally, we show in Fig. 15 the variation of the weighted bulk modulus of the void, $\bar{\lambda}^{v}$, as a function of the degree of saturation for the example with decreasing suction. The relevant phase relationships are as follows. At the end of each time increment the void ratio is obtained as $e = c(\xi)[N - \tilde{\lambda}\ln(-\bar{p}_{c})] - 1$, from which the volume fractions are then calculated. The elastic bulk modulus of water is taken as 2.2×10^{7} kPa [58], whereas the bulk modulus of air is taken as the air pressure p_{a} itself. The variation of p_{a} is assumed to follow Boyle–Mariotte's law for isothermal deformation, $p_{a}V_{a}$=constant, which means that the

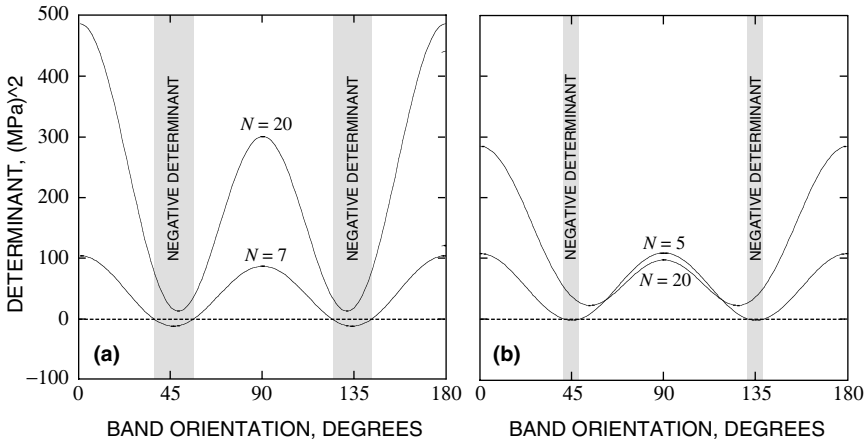

Fig. 14. Variation of determinant function with band orientation, $\beta = 0.50$: (a) undrained bifurcation near the critical state at constant suction; (b) undrained bifurcation near the critical state at decreasing suction.

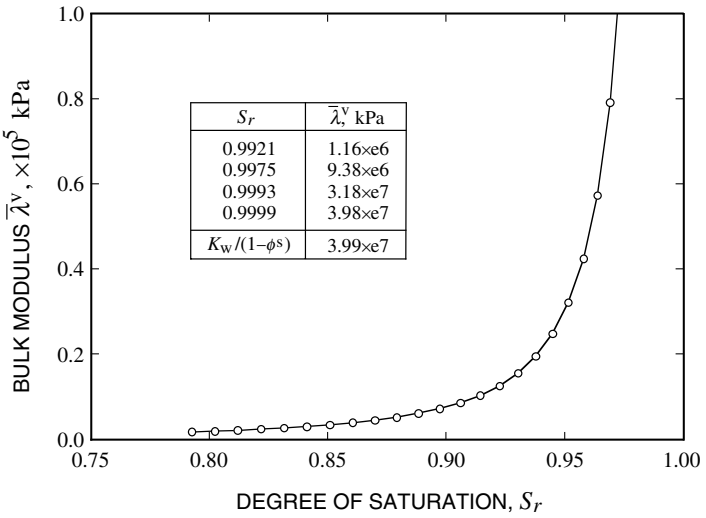

Fig. 15. Weighted bulk modulus of void versus degree of saturation for locally undrained deformation simulation.

air pressure increases as the air volume decreases. Since the volume of air is $V_a = \phi^a(1 + \epsilon_v)V_0$, where V_0 is the initial volume of the solid matrix and $\epsilon_v = \mathrm{tr}(\boldsymbol{u})$ is the corresponding volumetric strain, then $p_a \propto [\phi^a(1 + \epsilon_v)]^{-1}$. For the sake of analysis, we assume $p_a = 200$ kPa initially. The results of Fig. 15 show the expected approach of $\bar{\lambda}^v$ to $K_w/(1 - \phi^s)$ as $S_r \to 1$. Note, however, that S_r needs to be very, very close to unity to get to this limit ($S_r = 0.99$ is not close enough). Theoretically, $K_a \to \inf$ as $S_r \to 1$, but even with $S_r = 0.99$ the modulus K_a is still much smaller than K_w. We recall that S_r cannot be exactly equal to unity due to trapped air bubbles as reflected by the value of the van Genuchten parameter $S_2 < 1.0$. We also recall that in undrained deformation analysis of fully saturated media, $\bar{\lambda}^v$ is used as a 'penalty parameter' to impose the incompressibility constraint [66]. However, in the presence of air voids this parameter may not attain a large enough value which could result in a volume change of the mixture consistent with the compressibility of the solid skeleton as well as that of the air voids.

6. Closure

We have presented a mathematical framework for three-phase deformation and strain localization analyses of partially saturated porous media. Conservation laws have been used to identify energy-conjugate variables for constitutive model formulation. Using this framework we have cast a specific Cam-Clay-type plasticity model for partially saturated soils and implemented it numerically using the standard return mapping algorithm of computational plasticity. The implementation is remarkably simple and very much similar to that used for the fully saturated formulation [34]. Numerical examples were run to demonstrate the efficiency of the algorithm as well as the significant influence of the matrix suction, treated as an additional strain-like variable, on the deformation and strain localization responses of three-phase media. Results of these studies may be used to cast other, more robust constitutive models for partially saturated soils within the proposed framework, such as those involving all three invariants of the stress tensor.

Acknowledgments

The author is grateful to Professor Nasser Khalili of The University of New South Wales for enlightening discussions pertaining to partially saturated soils and for his unsolicited written review of the original draft of this paper; to Professor Bernhard Schrefler of University of Padua for discussions pertaining to the definition of effective stress in partially saturated soils; to two anonymous reviewers for their expert reviews and constructive comments; and to José Andrade and Gerhard Oettl of Stanford University for reading the preliminary draft of this manuscript. This work has been supported in part by National Science Foundation under Grant No. CMS-0201317, under the direction of Dr. C.S. Astill.

References

[1] J.A. Tindall, J.R. Kunkel, Unsaturated Zone Hydrology, Prentice-Hall, Upper Saddle River, NJ, 1999.
[2] G. Oettl, R.F. Stark, G. Hofstetter, A coupled three-phase FE-model for dewatering of soils by means of compressed air, Comput. Assis. Mech. Eng. Sci. 10 (2003) 1–22.
[3] G. Oettl, R.F. Stark, G. Hofstetter, Application of a coupled solid–fluid model to tunnelling, in: E. Oñate, D.R.J. Owen (Eds.), VII International Conference on Computational Plasticity, COMPLAS 2003, CIMNE, Barcelona, in CD Rom.
[4] H.R. Thomas, Editorial, Géotechnique 53 (2003) 1.
[5] D.G. Fredlund, N.R. Morgenstern, Stress state variables for unsaturated soils, J. Geotech. Engrg. Div. ASCE 103 (1977) 354–358.
[6] E.E. Alonso, A. Gens, A. Josa, A constitutive model for partially saturated soils, Géotechnique 40 (1990) 405–430.
[7] A. Gens, E. Alonso, A framework for the behaviour of unsaturated expansive clays, Can. Geotech. J. 29 (1992) 1013–1032.
[8] S.J. Wheeler, V. Sivakumar, An elasto-plastic critical state framework for unsaturated soil, Géotechnique 45 (1995) 35–53.
[9] J. Vaunat, J.C. Cante, A. Ledesma, A. Gens, A stress point algorithm for an elastoplastic model in unsaturated soils, Int. J. Plasticity 16 (2000) 121–141.
[10] A.W. Bishop, The principle of effective stress, Teknisk Ukeblad 39 (1959) 859–863.
[11] A.W. Bishop, G.E. Blight, Some aspects of effective stress in saturated and partly saturated soils, Géotechnique 13 (1963) 177–197.
[12] B. Loret, E. Rizzi, Strain localization in fluid-saturated anisotropic elastic–plastic porous media with double porosity, J. Mech. Phys. Solids 47 (1999) 503–530.
[13] B. Loret, N. Khalili, A three-phase model for unsaturated soils, Int. J. Numer. Anal. Meth. Geomech. 24 (2000) 893–927.
[14] B. Loret, N. Khalili, An effective stress elastic–plastic model for unsaturated porous media, Mech. Mater. 34 (2002) 97–116.
[15] G. Gallipoli, A. Gens, R. Sharma, J. Vaunat, An elasto-plastic model for unsaturated soil incorporating the effects of suction and degree of saturation on mechanical behaviour, Géotechnique 53 (2003) 123–135.
[16] S.M. Springman, C. Jommi, P. Teysseire, Instabilities on moraine slopes induced by loss of suction: a case history, Géotechnique 53 (2003) 3–10.
[17] D.J. Henkel, A.W. Skempton, A landslide at Jackfield, Shropshire, in a heavily over-consolidated clay, Géotechnique 5 (1955) 131–137.
[18] E.W. Brand, J. Premchitt, H.B. Phillipson, Relationship between rainfall and landslides in Hong Kong, Proc. 4th Int. Symp. Landslides 1 (1984) 377–384.
[19] T.T. Lim, H. Rahardjo, M.F. Chang, D.G. Fredlund, Effect of rainfall on matric suctions in a residual soil slope, Can. Geotech. J. 33 (1996) 618–628.
[20] C.W.W. Ng, Q. Shi, Influence of rainfall intensity and duration on slope stability in unsaturated soils, Quart. J. Engrg. Geol. 31 (1998) 105–113.
[21] J.W. Rudnicki, J.R. Rice, Conditions for the localization of deformation in pressure-sensitive dilatant materials, J. Mech. Phys. Solids 23 (1975) 371–394.
[22] R.I. Borja, A. Aydin, Computational modeling of deformation bands in granular media. I. Geological and mathematical framework, Comput. Methods Appl. Mech. Engrg. 193 (2004) 2667–2698.
[23] R.I. Borja, Computational modeling of deformation bands in granular media. II. Numerical simulations, Comput. Methods Appl. Mech. Engrg. 193 (2004) 2699–2718.
[24] J.W. Rudnicki, A formulation for studying coupled deformation pore fluid diffusion effects on localization of deformation, in: S. Nemat-Nasser (Coord.), Geomechanics, AMD-vol. 57, The American Society of Civil Engineers, New York, NY 1983, pp. 35–44.
[25] J.R. Rice, On the stability of dilatant hardening for saturated rock masses, J. Geophys. Res. 80 (1975) 1531–1536.

[26] J.R. Rice, D.A. Simons, The stabilization of spreading shear faults by coupled deformation-diffusion effects in fluid infiltrated porous materials, J. Geophys. Res. 81 (1976) 5322–5334.
[27] K. Terzaghi, Theoretical Soil Mechanics, John Wiley and Sons, New York, NY, 1943.
[28] A. Nur, J.D. Byerlee, An exact effective stress law for elastic deformation of rock with fluids, J. Geophys. Res. 76 (1971) 6414–6419.
[29] O. Zienkiewicz, C. Chang, P. Bettess, Drained, undrained, consolidating and dynamic behaviour assumptions in soils, Gétotechnique 30 (1980) 385–395.
[30] W. Ehlers, T. Graf, Adaptive computation of localization phenomena in geotechnical applications, in: J.F. Labuz, E. Drescher (Eds.), Bifurcation and Instabilities in Geomechanics, A.A. Balkema, Lisse, 2003, pp. 247–262.
[31] O. Coussy, Mechanics of Porous Continua, J. Wiley and Sons, New York, NY, 1995.
[32] D. Peric, M.A. Ayari, Influence of Lode's angle on the pore pressure generation in soils, Int. J. Plasticity 18 (2002) 1039–1059.
[33] D. Peric, A.M. Ayari, On the analytical solutions for the three-invariant Cam clay model, Int. J. Plasticity 18 (2002) 1061–1082.
[34] R.I. Borja, C. Tamagnini, Cam-Clay plasticity. Part III: Extension of the infinitesimal model to include finite strains, Comput. Methods Appl. Mech. Engrg. 155 (1998) 73–95.
[35] R.I. Borja, C. Tamagnini, A. Amorosi, Coupling plasticity and energy-conserving elasticity models for clays, J. Geotech. Geoenviron. Engrg. ASCE 123 (1997) 948–957.
[36] A. Schofield, P. Wroth, Critical State Soil Mechanics, McGraw-Hill, New York, 1968.
[37] K.H. Roscoe, J.H. Burland, On the generalized stress–strain behaviour of 'wet' clay, in: J. Heyman, F.A. Leckie (Eds.), Engineering Plasticity, Cambridge University Press, Cambridge, 1968, pp. 535–609.
[38] R.I. Borja, S.R. Lee, Cam-Clay plasticity. Part I: Implicit integration of elasto-plastic constitutive relations, Comput. Methods Appl. Mech. Engrg. 78 (1990) 49–72.
[39] R.I. Borja, Cam-Clay plasticity. Part II: Implicit integration of constitutive equation based on a nonlinear elastic stress predictor, Comput. Methods Appl. Mech. Engrg. 88 (1991) 225–240.
[40] L.E. Malvern, Introduction to the Mechanics of a Continuous Medium, Prentice-Hall, Inc., Englewood Cliffs, NJ, 1969.
[41] G.T. Houlsby, The work input to an unsaturated granular material, Géotechnique 47 (1997) 193–196.
[42] J.E. Marsden, T.J.R. Hughes, Mathematical Theory of Elasticity, Dover Publications, Inc., New York, NY, 1983.
[43] R.I. Borja, E. Alarcón, A mathematical framework for finite strain elastoplastic consolidation. Part 1: Balance laws, variational formulation, and linearization, Comput. Methods Appl. Mech. Engrg. 122 (1995) 145–171.
[44] B.A. Schrefler, The finite element method in soil consolidation (with applications to surface subsidence), Ph.D. Thesis, University College of Swansea, C/Ph/76/84, 1984.
[45] R.W. Lewis, B.A. Schrefler, The finite element method in the deformation and consolidation of porous media, J. Wiley and Sons, Chichester, 1987.
[46] G.T. Houlsby, The work input to a granular material, Géotechnique 29 (1979) 354–358.
[47] R.J. Atkin, R.E. Craine, Continuum theories of mixtures: Basic theory and historical development, Quart. J. Mech. Appl. Math. 29 (1976) 209–244.
[48] R.M. Bowen, Theory of mixtures, in: A.C. Eringen (Ed.), Continuum Physics, vol. III—Mixtures and EM Field Theories, Academic Press, New York, 1976, pp. 1–127.
[49] R.I. Borja, Conservation laws for three-phase partially saturated granular media, Proceedings of the International Conference from Experimental Evidence Towards Numerical Modelling of Unsaturated Soils, Weimar, Germany, 18–19 September 2003.
[50] M.A. Biot, Nonlinear semilinear rheology of porous solids, J. Geophys. Res. 78 (1973) 4924–4937.
[51] R. Hill, The Mathematical Theory of Plasticity, Oxford University Press, Oxford, UK, 1950.
[52] J.C. Simo, T.J.R. Hughes, Computational Inelasticity, Springer-Verlag, New York, NY, 1998.
[53] S.J. Wheeler, D. Gallipoli, M. Karstunen, Comments on the use of Barcelona Basic Model for unsaturated soils, Int. J. Numer. Anal. Methods Geomech. 26 (2002) 1561–1571.
[54] D. Sheng, Non-convexity of the Barcelona Basic Model—Comment on S.J. Wheeler, D. Gallipoli and M. Kastunen (2002;26:1561–1571), Int. J. Numer. Anal. Methods Geomech. 27 (2003) 879–881.
[55] J.R. Rice, J.W. Rudnicki, A note on some features of the theory of localization of deformation, Int. J. Solids Struct. 16 (1980) 597–605.
[56] R.N. Brooks, A.T. Corey, Properties of porous media affecting fluid flow, J. Irrigation Draining Div. ASCE 92 (1966) 61–68.
[57] M.Th. van Genuchten, A closed-form equation for predicting the hydraulic conductivity of unsaturated soils, Soil Sci. Soc. Am. J. 44 (1980) 892–898.
[58] D. Halliday, R. Resnick, J. Walker, Fundamentals of Physics, Sixth ed. (Extended), John Wiley and Sons, New York, NY, 2001.
[59] J. Bear, Dynamic of Fluids in Porous Media, Dover Publications, Inc., New York, 1972.
[60] R. de Boer, Theory of Porous Media, Springer-Verlag, Berlin, Germany, 2000.

[61] W. Ehlers, Foundations of multiphase and porous materials, in: W. Ehlers, J. Bluhm (Eds.), Porous Media: Theory: Experiments and Numerical Applications, Springer-Verlag, Berlin, 2002, pp. 3–86.
[62] R.I. Borja, Bifurcation of elastoplastic solids to shear band mode at finite strain, Comput. Methods Appl. Mech. Engrg. 191 (2002) 5287–5314.
[63] G.T. Houlsby, The use of a variable shear modulus in elastic–plastic models for clays, Comput. Geotech. 1 (1985) 3–13.
[64] R. Butterfield, A natural compression law for soils, Géotechnique 29 (1979) 469–480.
[65] R.A. Fisher, On the capillary forces in an ideal soil; correction of formulae given by W.B. Haines, J. Agricult. Sci. 16 (1926) 492–505.
[66] T.J.R. Hughes, The Finite Element Method, Prentice-Hall, Englewood Cliffs, New Jersey, 1987.